Limnol. Oceanogr., 59(6), 2014, 1805–1838
© 2014, by the Association for the Sciences of Limnology and Oceanography, Inc.
doi:10.4319/lo.2014.59.6.1805

Stratification and horizontal exchange in Lake Victoria, East Africa

Sally MacIntyre,[1,2,*] José R. Romero,[1,4,a] Gregory M. Silsbe,[5,b] and Brian M. Emery [1,3]

[1] Earth Research Institute, University of California, Santa Barbara, California
[2] Department of Ecology, Evolution, and Marine Biology, University of California, Santa Barbara, California
[3] Marine Science Institute, University of California, Santa Barbara, California
[4] Centre for Water Research, University of Western Australia, Crawley, Western Australia, Australia
[5] Department of Biology, University of Waterloo, Waterloo, Ontario, Canada

Abstract

We characterize stratification patterns over diel, seasonal, and annual time scales in inshore and offshore regions of Lake Victoria, East Africa; determine conditions leading to horizontal exchanges; and, using surface energy budgets derived from local meteorological stations and two reanalysis products, address whether stratification depends on advective as opposed to local processes. The largest change in the surface energy budget occurred when winds intensified at the end of the long rains, with the wind's intensification, duration, and spatial extent dependent on El Niño–Southern Oscillation cycles. These winds flush inshore waters and cause cross-basin upwelling similar to that observed in the deep African Great Lakes. Wedderburn numbers indicated mixing and cross-basin within-thermocline transport. The internal wave-induced mixing and enhanced latent heat fluxes of -300 to -400 W m^{-2} contributed to the loss of seasonal stratification. Advection of cool water was required to balance the heat budget of northern offshore waters in the latter half of the southeast monsoon except in an El Niño year. Northern waters became weakly stratified after the southeast monsoon, with nocturnal winds contributing to heat transport and ventilation of the lower water column. Following the rainy season, downwelling by sustained southerly albeit low winds is a likely cause of the seasonal thermocline. Inshore waters are 0.2–1.5°C warmer than those offshore, conditions conducive to horizontal convective circulation except during onshore winds. The seasonal cycle of stratification and inshore–offshore and cross-basin exchanges are moderated by differential heating, cooling, and basin-scale thermocline tilting.

The diel, seasonal, and annual variations in stratification within lakes influence the magnitude of vertical mixing, inshore–offshore exchanges, persistence of hypoxia, fluxes of greenhouse gases and nutrients, and the timing and duration of phytoplankton growth, with consequences for higher trophic levels. The variations in temperature and stratification depend on the surface energy budget, that is, the net shortwave and longwave radiation and sensible and latent heat fluxes combined with advection and the input of momentum from winds. Surface energy budgets are powerful tools for understanding controls on latitudinal variations in lake thermal structure and for quantifying how the energy inputs and water losses from lakes vary with changes in climate (Lenters et al. 2005; MacIntyre and Melack 2009; Liu et al. 2011). Further, when obtained in combination with time-series measurements of water temperatures, they can be used to quantify turbulence within the upper mixing layer (Imberger 1985; MacIntyre et al. 2010) and to determine the importance of heat loss vs. wind in generating turbulence with consequences, for instance, for depth and timing of vertical mixing and evasion of greenhouse gases (MacIntyre et al. 2002; Read et al. 2012). For lakes large enough for spatial variations in surface meteorology, surface energy budgets can be used to compute the likelihood of horizontal exchanges driven by spatial differences in temperatures (Verburg et al. 2011; Cozar et al. 2012).

Quantifying the surface energy budgets of tropical African lakes and the resulting thermal structure, extent of vertical mixing, and horizontal exchanges is particularly important given the ongoing eutrophication in the context of climate change (Hecky et al. 2010; Otu et al. 2011; Wolff et al. 2011). For example, the shift from mesotrophy to eutrophy in Lake Victoria (Hecky et al. 2010) coincided with a several-year period of reduced latent heat fluxes at the time of a phase shift in the Pacific Decadal Oscillation (MacIntyre 2013) and a step change in sea surface temperature in the Indian Ocean and other tropical oceans (Clark et al. 2003). Our understanding of stratification dynamics and surface energy budgets in the East African Great Lakes is based on a modest number of time-series temperature measurements and meteorological measurements, with these efforts reviewed in Spigel and Coulter (1996), Talling and Lemoalle (1998), and MacIntyre (2013). A mechanistic understanding of how the surface energy budget and wind drive the hydrodynamics of Lake Victoria is required to predict ecosystem-level changes and for fisheries management (Kolding et al. 2008; Cozar et al. 2012).

The annual cycle of stratification in tropical lakes is caused by seasonal changes in cloud cover as it affects net shortwave and longwave radiation and by seasonal changes in wind speed as it affects momentum fluxes and, in

* Corresponding author: sally@eri.ucsb.edu

Present addresses:
[a] GHD, Perth, Western Australia, Australia
[b] Centre for Marine and Estuarine Research, Netherlands Institute of Ecology, Yerseke, Netherlands

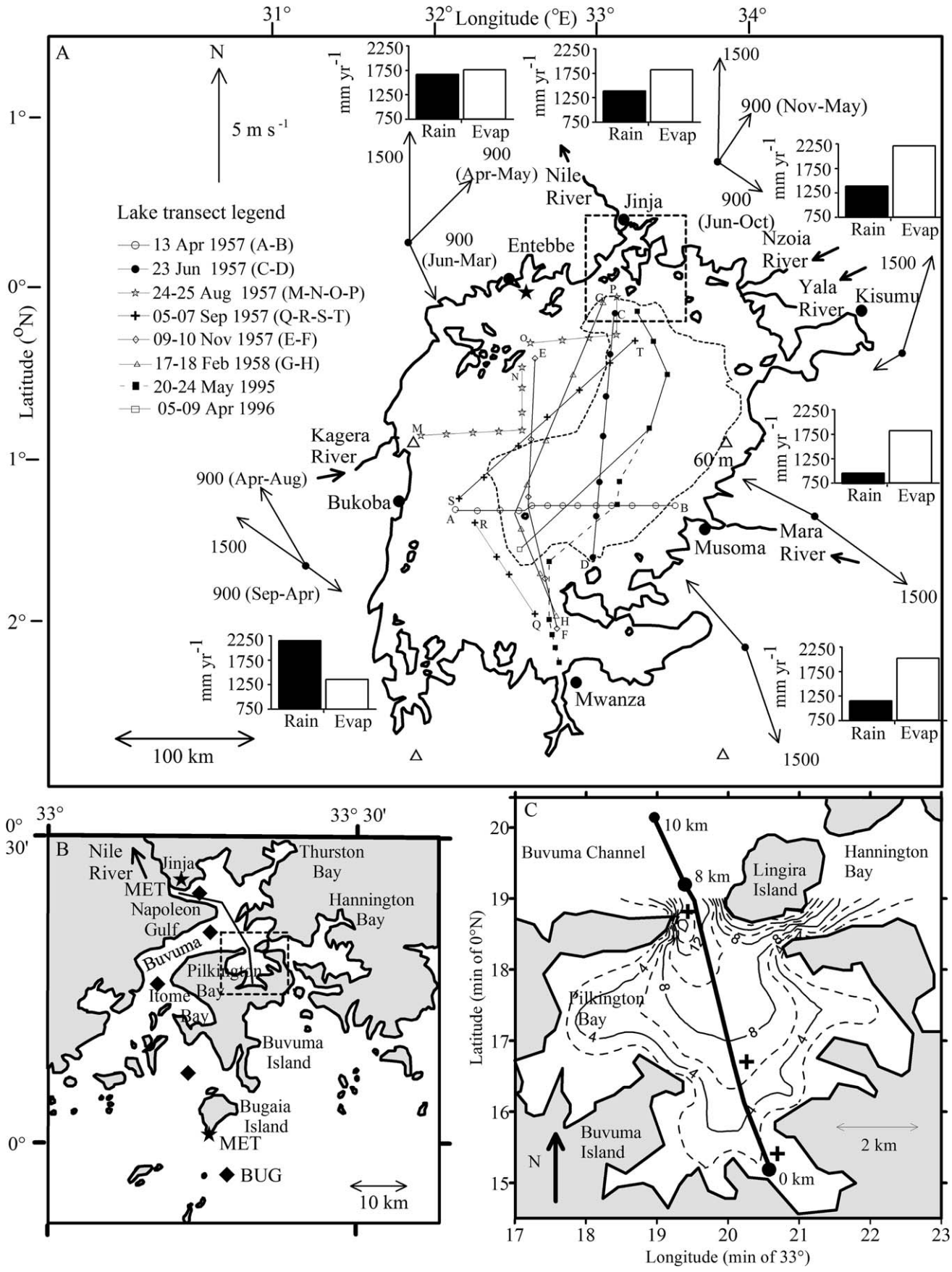
A
N
5 m s -1
Lake transect legend
13 Apr 1957 (A-B)
23 Jun 1957 (C-D)
24-25 Aug 1957 (M-N-O-P)
05-07 Sep 1957 (Q-R-S-T)
09-10 Nov 1957 (E-F)
17-18 Feb 1958 (G-H)
20-24 May 1995
05-09 Apr 1996
Longitude (°E)
Latitude (°N)
31°
32°
33°
34°
1°
0°
2°
Nile River
Jinja
Entebbe
Nzoia River
Yala River
Kisumu
Kagera River
Bukoba
Musoma
Mara River
Mwanza
60 m
100 km
900 (Apr-May)
900 (Nov-May)
900 (Jun-Oct)
900 (Jun-Mar)
900 (Apr-Aug)
900 (Sep-Apr)
1500
mm yr -1
2250
1750
1250
750
Rain
Evap
B
33°
33° 30'
0° 30'
0°
Nile River
Jinja
MET
Napoleon Gulf
Thurston Bay
Hannington Bay
Buvuma
Pilkington Bay
Itome Bay
Buvuma Island
Bugaia Island
MET
BUG
10 km
C
Buvuma Channel
10 km
8 km
0 km
Lingira Island
Hannington Bay
Pilkington Bay
Buvuma Island
N
2 km
Latitude (min of 0°N)
Longitude (min of 33°)
20
19
18
17
16
15
17
18
19
20
21
22
23

combination with relative humidity, latent heat fluxes (Talling and Lemoalle 1998). These variables predominate because of the more muted variability in solar radiation and air temperature in the tropics relative to higher latitudes. With their warm temperatures, evaporation rates can exceed those of temperate or arctic lakes for the same wind speed, causing greater mixed-layer deepening (MacIntyre and Melack 2009). The high evaporation rates contribute towards diel stratification and mixing being a dominant characteristic of tropical lakes (Talling 1957; Melack and Kilham 1974; MacIntyre and Melack 1982). Stratification can also be caused by differential cooling, the process in which gravity currents are induced by greater cooling in shallow or sheltered regions and subsequently flow offshore (Talling 1963). Within the tropics, large-scale climate drivers that influence the movement of the Intertropical Convergence Zone (ITCZ) influence seasonal and interannual variability in surface energy budgets. Paleo-studies indicate that this variability influences the duration of seasonal wind-driven mixing (Wolff et al. 2011).

Talling (1963) suggested that horizontal convective exchanges would occur in numerous weakly stratified tropical lakes and that identifying density-driven flows would be particularly challenging in Lake Victoria with its large size and complex shoreline. Density-driven flows occur if there are spatial differences in rates of heating and cooling due to variable depth, wind exposure, or, in the case of large lakes, differences in climate around the lake (Monismith et al. 1990; Wells and Sherman 2001; Verburg et al. 2011). Flows due to differential cooling have been observed in Lake Albert (Talling 1963) and the southern basin of Lake Malawi (Eccles 1974; Patterson et al. 1998). Horizontal convective circulation as in Imberger (1974) has been identified in Lake Tanganyika by Verburg et al. (2011). This circulation, induced by greater heating to the north than to the south, persists for several months and operates as a conveyor belt with southerly flow in the surface layer in opposition to wind-induced currents and northerly flow in the thermocline. Cozar et al. (2012), using remotely sensed data in combination with computed monthly surface energy budgets for the northern and southern basins of Lake Victoria, inferred that horizontal convective circulation occurs within the lake for approximately 2 months near the end of the southeast monsoon. East–west differences in surface energy budgets that could induce horizontal exchanges in surface waters may also result in Lake Victoria because of the greater cloud cover (Yin et al. 2000) and shallower morphometry to the west. With respect to inshore waters, if they are consistently warmer than those farther offshore, horizontal convective exchanges similar to those analyzed by Burling et al. (1999) and Ivey (2004) may result. If, over diel timescales, inshore waters are alternately warmer and cooler than those farther offshore, alteration of buoyant overflows and negatively buoyant underflows would result (Monismith et al. 1990; Farrow and Patterson 1993). Thus, exchanges due to horizontal temperature differences are anticipated over large and small spatial scales in Lake Victoria.

An additional challenge for Lake Victoria is to determine whether the presumed over- or underflows would persist or dominate given the other physical processes operative within the lake. With high latent heat fluxes, vertical mixing could disrupt or lessen the mass transfer possible from exchange flows (Ivey 2004; Bednarz et al. 2009) and wind-induced circulation could overwhelm them. For example, gyres (Kitaka 1971; Song et al. 2002) could predominate over horizontal convection on the basin scale and internal waves or flushing on the embayment scale (Fish 1957; Newell 1960). Assessment of the dominant exchange mechanisms in Lake Victoria in the context of larger-scale meteorology will contribute to our understanding of interannual variability in ecosystem processes.

In the following, we present results of a study of the physical limnology of Lake Victoria conducted from 1994 to 1996 and designed to develop a mechanistic understanding of the stratification and exchange dynamics of the lake. Our interpretations are extended by analysis and synthesis of earlier studies and by two lakewide synoptic surveys obtained in 2000. We illustrate diel, seasonal, and spatial variability of surface meteorological forcing using data from six inshore sites around the lake, with half-hour average data from a meteorological station alternately placed at inshore and offshore locations at the northwestern end of the lake, 6 h modeled National Centers for Environmental Prediction

←

Fig. 1. (A) Map of the shoreline and 60 m isobath of Lake Victoria illustrating the major riparian cities, major rivers (Kagera, Nzoia, Yala, Mara) and the Nile River outlet at Owen Falls Dam near Jinja. Nyanza Gulf is the embayment to the south of Kisumu. Recent (May 1995, April 1996) and historical (April 1957–February 1958) transect stations across the main basin are shown. The northern portion of the transect in April 1996 is the same as that in May 1995. For each riparian city the mean annual totals of evaporation (Evap) and rainfall (Rain) for 1969–1983, and average morning (09:00 h) and afternoon (15:00 h) wind speeds and directions for 1958–1969 are summarized. The three western meteorological (MET) stations had different morning wind directions for some period of the year as noted in the figure. The convention for the wind vector plots is the direction of travel of the wind. (B) Enlargement of the northern region of the lake showing the inshore to offshore transect stations (diamond), the Bugaia offshore station (BUG), and the diurnal Napoleon Gulf (near Nile outlet) to Pilkington Bay transect (line). (C) Enlargement of Pilkington Bay showing the 2 m isobath intervals, transect of the diel inshore studies, and locations of drogue current measurements (cross) during May and June 1996. Locations of meteorological station deployments (star; A) for the FTI near Entebbe (December 1994–February 1995) and (B) for Jinja (July–November 1994, February 1995–June 1996) and Bugaia Island (June 1994). (A) Star also marks position of NCEP reanalysis data at global grid point 1 (0°, 32.5°E); open triangles indicate Gaussian grid points 1 (0.9524°S, 31.875°E), 3 (0.9524°S, 33.75°E), 2 (−2.8571°S, 31.875°E), and 4 (−2.8571°S, 33.75°E). ERA-I grid points 1 (0.0°S, 32.25°E), 2 (0.0°S, 33°E), 3 (0.00°S, 33.75°E), 4 (0.75°S, 32.25°E), 5 (0.75°S, 33°E), 6 (0.75°S, 33.75°E), 7 (1.5°S, 32.25°E), 8 (1.5°S, 33.0°E), 9 (1.5°S, 33.75°E), 10 (2.25°S, 32.25°E), 11 (2.25°S, 33.0°E), 12 (2.25°S, 33.75°E; not shown).

(NCEP)/National Center for Atmospheric Research reanalysis data (Kalnay et al. 1996) for four grid points on or adjacent to the lake (Fig. 1A), and 6 h modeled surface and 12 h modeled radiation data from the European Center for Medium-Range Weather Forecasts (ECMWF) ERA-Interim (ERA-I; Dee et al. 2011) at 12 grid points on the lake. The data from the six inshore meteorological stations were collected intermittently and illustrate spatial variability; between-year variability is lost because of the necessity for averaging. In contrast, the modeled reanalysis data are spatially averaged but illustrate temporal variability over 6 h time scales. A challenge is to determine verifiable patterns given the shortcomings of the two types of data. Temporal variability in thermal structure was quantified by time-series measurements at a northern offshore station near that where previous time-series measurements were obtained; spatial and temporal variability in thermal structure was quantified by whole lake spatial surveys and by cross-basin transects. Spatial and temporal variability in the northern archipelago was quantified by transects between inshore and offshore waters and across inshore embayments. With these combined data sets we assess how surface meteorology and basin morphometry create temporal and spatial differences in thermal structure. We use scaling analyses to determine whether vertical mixing would disrupt predicted horizontal exchanges. This mechanistic analysis sets the stage for subsequent efforts to quantify how changes in land use and climate contribute to the observed warming and hypoxia within Lake Victoria (Hecky 1993; Hecky et al. 1994; Bugenyi and Magumba 1996).

Study site

Lake Victoria (0.5°N–3°S, 31.5–34.5°E) is the world's second largest freshwater and the largest tropical lake in terms of surface area (68,800 km^2), but it is shallow (maximum depth of 79 m, average depth of 40 m) relative to many other great lakes and has a highly indented shoreline with numerous islands, bays, channels, and wetlands (Fig. 1A). The five major inshore archipelagos around the lake perimeter include the Jinja, Uganda, region in the north; the Entebbe-Sesse Island, Uganda, region of the northwest; the southwestern corner of the lake in Tanzania; the Speke Gulf-Mwanza-Ukerewe Island, Tanzania, region in the southeast; and Nyanza (Winam, Kavirondo) Gulf, Kenya, in the northeast. External loading from land use change has resulted in eutrophication (Hecky 1993; Verschuren et al. 2002). Precipitation dominates over river inflows in the water budget of the lake (Gikumu-Njuru et al. 2013).

The meteorology over Lake Victoria is structured by the presence or absence of the southeast winds from the Indian Ocean that generally begin in May and end in August (Schott and Fernandez-Partagas 1981) and two rainy seasons, the long rains from March to May and the short rains from October to December, whose timing varies spatially around the lake (Nicholson and Yin 2002). Atmospheric attenuation of insolation varies over the lake because of gradients of moisture in the atmospheric boundary layer (Monteith 1972); similarly, humidity increases from the south to the north such that evaporation is higher to the south (Newell 1960). Descriptions of the physical limnology of Lake Victoria have been based on studies that include seasonal monitoring of an offshore station in the northern main basin with transects to inshore channels during 1952–1953 (Fish 1957) and 1960–1961 (Talling 1966), temperature transects across the main basin of Lake Victoria during 1957–1958 (Newell 1960), and lakewide bottom temperatures obtained during September 1927 (Graham 1929), as well as several studies of the dynamics of inshore waters summarized in Crul (1995). These previous studies and the consequences to the ecology of the African Great Lakes are summarized in Beadle (1981), Crul (1995), and Talling and Lemoalle (1998).

Lake Victoria is monomictic with a three-phase stratification regime developed for northern offshore waters (Talling 1966). After holomixis, phase 1 occurs from September to December and is marked by surface warming and small thermal gradients over most of the water column. A well-defined seasonal mixed layer with a deep thermocline characterizes phase 2 from January to May. Phase 3 (June–August) is characterized by occasional holomixis, but generally small vertical temperature differences occur throughout the water column. Although these phases are influenced by seasonal meteorological patterns, the linkages made so far have not been made explicit with a surface energy budget.

Methods

Meteorology—Monthly averaged wind speed and direction, air temperature, relative humidity, and cloud fraction for the period 1958–1969 (Meteorological Department of the East African High Commission [MDEAHC] 1959, 1960, 1961, 1962, 1963, 1964, 1965, 1966, 1967, 1968, 1969, 1970) from six shoreline stations around the perimeter of Lake Victoria were used to characterize lakewide variability in meteorological forcing. Because of the intermittent data collection, averages are for the full period of record and are given for morning land breeze conditions (09:00 h) and afternoon (15:00 h) lake breeze conditions. Data collection was too intermittent at night to include nighttime values. Based on personal observations, anemometer height was 2 m. Solar radiation is available as monthly averages of daily integrated values from 1969 through 1983 (MDEAHC 1969–1983). Meteorological data are available from 1958 until the present from these same stations from the U. S. National Oceanographic and Atmospheric Administration. We also analyzed these data, but present results with the data from 1958 through 1969, when sampling was more consistent. Decadal averaging was still required because of variable periods of consistent sampling at the stations around the lake. All stations except Musoma had 5–8 years of data at the two times of day. The magnitudes of the more limited data from Musoma are within the range for monthly data over the longer time period. We deployed a meteorological station in the northwestern archipelago during 1994–1996. Measurements with this station included shortwave radiation (PSP, Eppley), photosynthetically active radiation (PAR; 190-SB, Li-Cor), wind speed (014A, Met One) and direction (024A, Met One) at 2 m height, air temperature and relative

Table 1. Sampling strategy for Lake Victoria. Unless otherwise stated, sampling occurred from June 1994 to June 1996. Secchi depth was measured at the Bugaia offshore station, on the two lakewide transects, on most of the inshore to offshore transects, and for most of the Pilkington Bay studies. Profiles of PAR were obtained throughout the northern archipelago, at the northern offshore station, and on the two lakewide transects.

Location	Procedure	Frequency	Instrumentation
Bugaia offshore station	Temperature, conductivity, and oxygen profiles (Fig. 1A,B)	Biweekly to bimonthly	SeaBird 19 and Hydrolab, water samples for Chl *a*
Main basin	North–south cross-basin transects, ~300 km (Fig. 1A)	Twice, Apr 1996 and May 1995	SeaBird 19 and Hydrolab, water samples for Chl *a*
Main basin (Newell 1960)	North–south and east–west cross-basin transects (Fig. 1A)	1957–1958, 6 transects	Reversing thermometer
Main basin	Synoptic sampling over 2 week period	Feb and Aug 2000	SeaBird 19
Bugaia Channel	Transects from Jinja to offshore station, ~60 km (Fig. 1B)	Monthly to bimonthly	SeaBird 19
Inshore region	Transects from Napoleon to Pilkington Bays (Fig. 1B,C)	4 times in 1994; 2 times per day	SeaBird 19
Pilkington Bay	Transects across Pilkington Bay into Buvuma Channel (Fig. 1C) 6–7 times over 1–2 diel cycles	4 times: May and Jun 1996; Nov 1995 (data not shown); Apr 1995 (MacIntyre et al. 2002)	SeaBird 19; Hydrolab 01–02 Nov 1995 and Jun 1996; drogues in Apr 1995 and May and Jun 1996

humidity with a radiation shield (HMP35C, Vaisalia), and rainfall (525, Texas Instruments). Data were obtained primarily at the Jinja pier in Napoleon Gulf (Fig. 1A,B) from June 1994 to June 1996, except for several brief deployments at Bugaia Island (June 1994; Fig. 1A,B) and the Fisheries Technological Institute (FTI) near Entebbe (December 1994–February 1995; Fig. 1A). Measurements were averaged over 30 min. Data from these stations allowed comparison of the inshore (Jinja) and offshore (Bugaia Island [1994], FTI [1995]) meteorological forcing of northern Lake Victoria. Daily meteorological measurements from 1994 to 1996 from the Uganda Water Development Department at a shoreline station in Entebbe, the outflow discharge to the Nile River at Owen Falls Dam, and lake level at Entebbe Pier were used to construct a water balance of the northwestern region over the study period. We obtained 6 h modeled NCEP reanalysis I data (Kalnay et al. 1996) and reanalysis II data (Kanamitsu et al. 2002) from one global grid point and three Gaussian grid points on or adjacent to Lake Victoria and ECMWF ERA-I (Dee et al. 2011) data for 12 grid points within the lake margin (caption, Fig. 1A).

Temperature, specific conductivity, dissolved oxygen, irradiance, and currents—Data were taken at fixed stations or on transects (Table 1). Temperature and conductivity profiles were obtained in 1994–1996 with a conductivity–temperature–depth (CTD) profiler (SBE-19, Sea-Bird Electronics) at a sampling rate of 2 Hz deployed in free-fall mode with a descent rate of 0.5 m s^{-1} (vertical resolution of 0.25 m). Specific conductivity (conductivity at 25°C, μS cm^{-1}) was calculated from temperature and conductivity measurements after correction for the slower thermistor response (time constant 0.5 s). Profiles of dissolved oxygen in 1994–1996 were obtained with a Hydrolab profiler. PAR was measured with a Li-Cor Spherical Quantum Sensor, and diffuse attenuation coefficients (k_d) were calculated using Beer's law. Samples for pigment analysis were filtered onto Whatman GFF filters in the field, stored in the dark and cold, and analyzed for chlorophyll *a* (Chl *a*; Stainton et al. 1977) on return to the lab. Currents were measured with drogues as in MacIntyre et al. (2002) at stations inshore, mid-bay, and in the connecting channel between Pilkington Bay and Buvuma Channel at two to five depths before and after CTD transects on 13–14 May and 03–04 June 1996 (Fig. 1C). Temperature profiles on whole-lake surveys in 2000 were measured with a SBE-19 CTD profiler. Sampling was conducted during the day, and each full survey took 2 weeks. Density was calculated from temperature with the international equation of state for seawater (Millero and Poisson 1981), as the contribution from dissolved salts to the water density is low (MacIntyre et al. 2002), and used to compute buoyancy frequency, $N = (g/\rho\ \partial\rho/\partial z)^{1/2}$, where g is gravity and ρ is density, and the magnitude of vertical overturns, that is, the vertical dimension of turbulent eddies, following Imberger (1985).

Calculations—Surface energy budgets were calculated following Imberger and Patterson (1990) and MacIntyre et al. (2002). Surface heat flux is the sum of latent and sensible heat and net longwave radiation, and net heat flux as reported here is the sum of surface heat flux and net shortwave radiation. Advection is also a term in a heat budget. As our field data do not include measurements of advection, we infer when heat was transported by comparing temperature changes computed from net heat flux and from integrated temperatures. We computed surface energy budgets using three distinct data sets: (1) the average monthly meteorological data from morning (09:00 h) and afternoon (15:00 h) at the six meteorological stations around the lake (Fig. 2), (2) our time-series

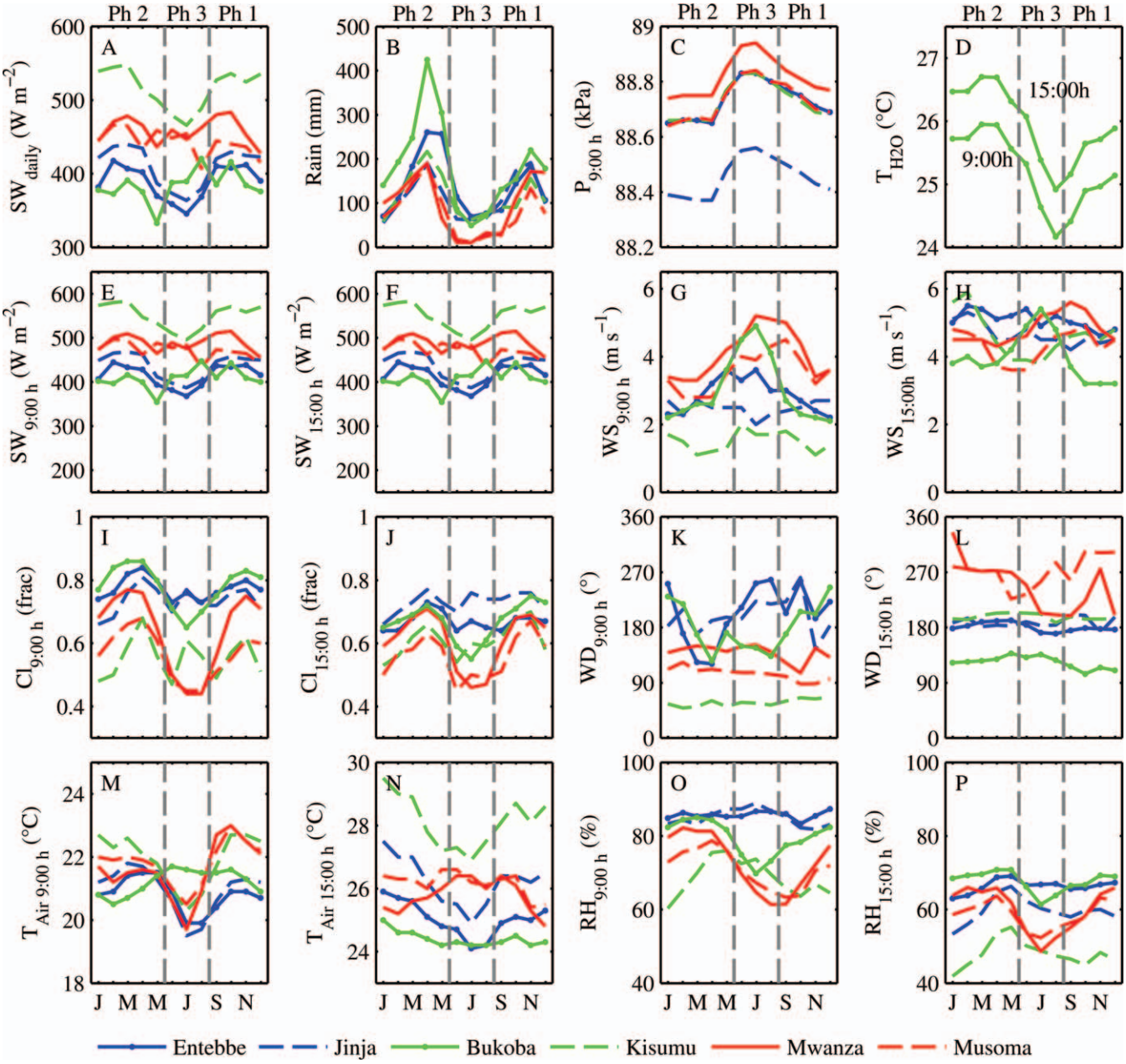

Fig. 2. Monthly averages at Entebbe, Jinja, Bukoba, Kisumu, Mwanza, and Musoma of (A) average shortwave radiation over 12 h (SW_{daily}); (B) total rainfall (Rain); (C) morning air pressure ($P_{09:00}$; no Bukoba data); (D) surface-water temperatures (T_{H2O}) for 09:00 h with 15:00 h 0.75°C higher at northern offshore station (Talling 1966); (E) 09:00 h and (F) 15:00 h estimated shortwave radiation (SW); (G) 09:00 h and (H) 15:00 h wind speed (WS); (I) 09:00 h and (J) 15:00 h fractional cloud cover (Cl); (K) 09:00 h and (L) 15:00 h wind direction (WD); (M) 09:00 h and (N) 15:00 h air temperature (T_{Air}); and (O) 09:00 h and (P) 15:00 h relative humidity (RH). Meteorological data are from 1958 through 1969, except for shortwave radiation, which was from 1969 through 1983. *See* Fig. 1 for locations of these shoreline sites around the perimeter of the lake. Vertical dashed lines delineate phases of stratification (Talling 1966).

measurements in inshore and offshore waters (Fig. 3), and (3) the reanalysis data (Fig. 4; Tables 2, 3). We selected three grid points from western locations to show north to south trends and one mid-basin grid point to illustrate conditions to the east with the NCEP reanalysis 1 data (Figs. 1A, 4). We did not use the data from the Gaussian grid point to the southeast given the larger land area included in the spatial averaging. Because of the sparse surface-water temperature data available, we conducted a sensitivity analysis to assess the error in our heat flux estimates.

Calculations: Monthly averaged meteorological data—We estimated net shortwave radiation for specific times of day from the available monthly averages of daily integrated data following Brock (1981) with the correction for albedo, taking into account angle of refraction, latitude, day of year, and time of day, with the latter three determining the

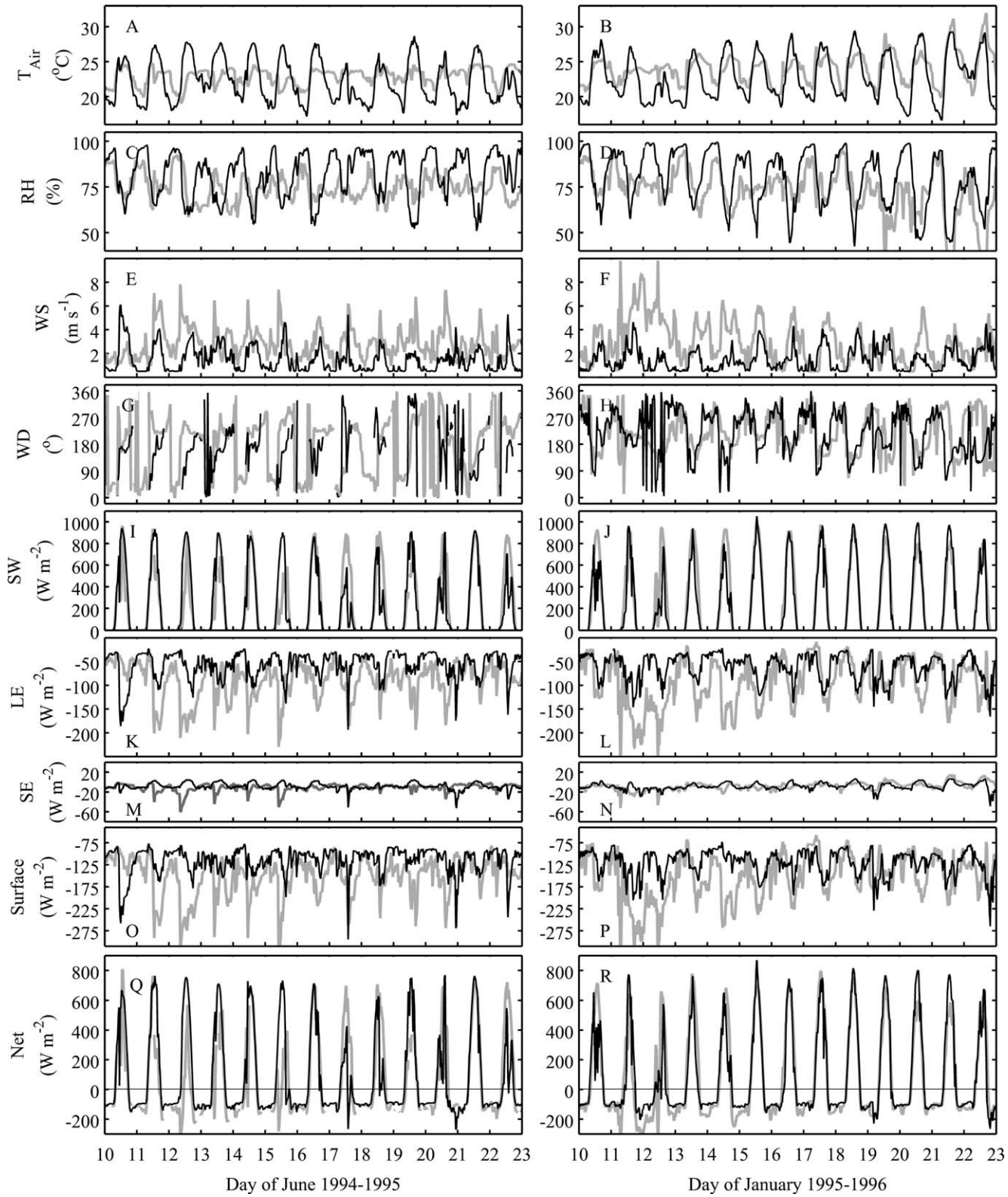

Fig. 3. Thirty minute averages over 13 d periods during (left panels) the southeast (mid-June) and (right panels) northeast monsoons (mid-January) of (A, B) air temperature; (C, D) relative humidity; (E, F) wind speed; (G, H) vector wind direction; (I, J) shortwave radiation; (K, L) latent (LE), (M, N) sensible (SE), (O, P) surface (surface = LE + SE + LW_{Net} where LW_{Net} is assumed equal to -50 W m^{-2}), and (Q, R) net energy fluxes (net = surface + SW_{Net}), with correction for albedo included in analysis, at the offshore stations (Bugaia, June 1994, and FTI, January 1995, gray lines) and over the same days but 1 year later at the northern inshore station at Jinja (black lines). Naming conventions for measured variables as in Fig. 2.

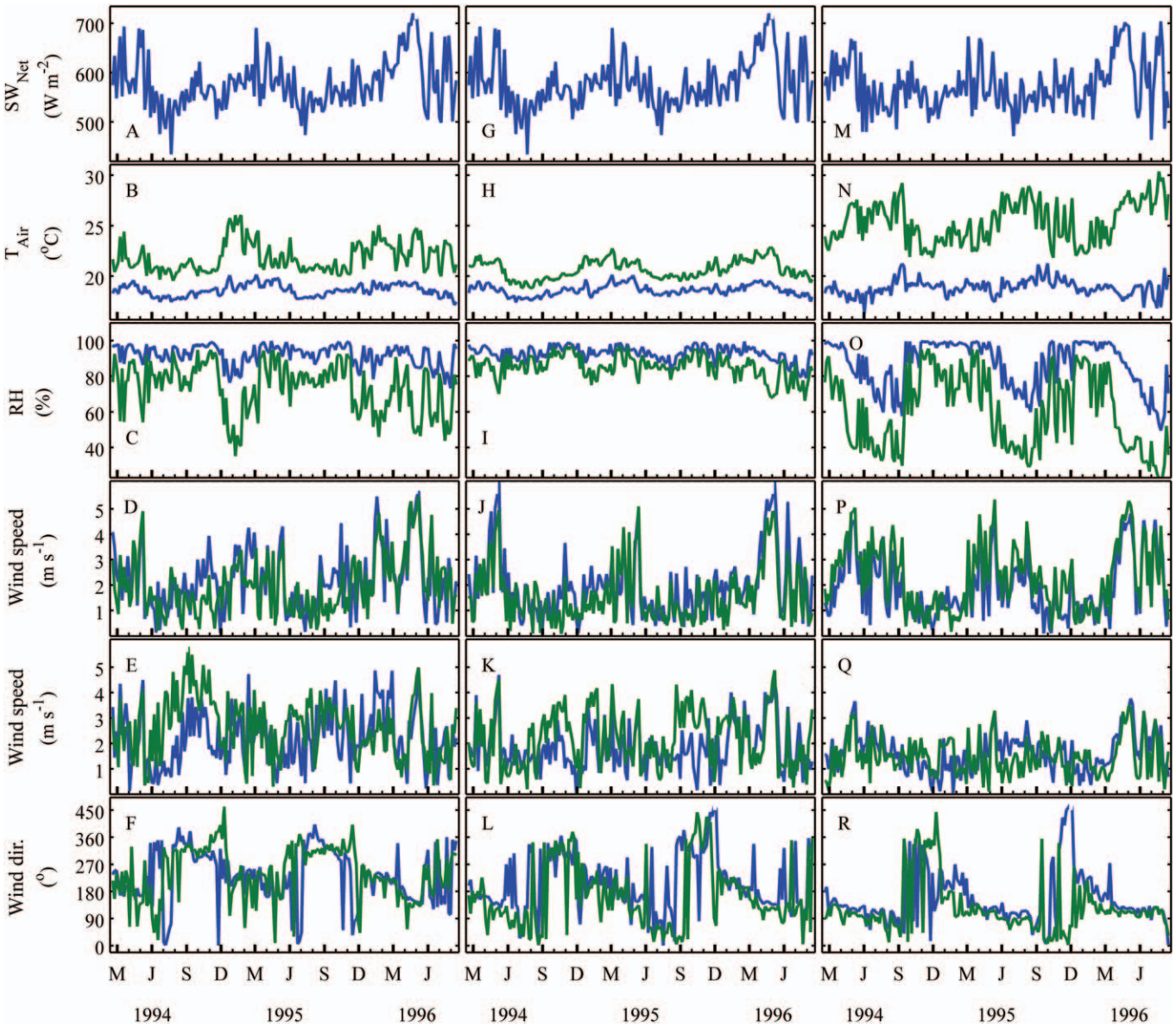

Fig. 4. Time series of 5 d averaged NCEP reanalysis 1 meteorological data (Fig. 1A) from (left panels) northern sector, global grid Point 1; (middle panels) mid-lake western sector, Gaussian grid point 1; and (right panels) southwestern sector, Gaussian grid point 2 from March 1994 through August 1996. Tick marks are centered mid-month. (A, G, M) Net shortwave radiation (SW_{Net}, average value 09:00 h to 15:00 h; data in (A) are from Gaussian grid point 1); (B, H, N) air temperature (09:00 h and 15:00 h); (C, I, O) relative humidity (09:00 h and 15:00 h); (D, J, P) wind speed (09:00 h and 15:00 h); (E, K, Q) wind speed (21:00 h and 03:00 h); (F, L, R) wind direction (09:00 h and 21:00 h). Blue lines in panels are the first of the two times.

zenith angle. Computation of net longwave radiation takes into account the reflection of 3% of incoming longwave radiation. Density of air, ρ_{air}, in kg m^{-3}, depends on air pressure, P; air temperature, T_{air}; and saturated specific humidity of the air, q_s. $\rho_{air} = 100P/(R_{gas}(T_{air} + 273.15)(1 + 0.608\ q_s))$, where P has units of 0.1 kPa, R_{gas} = 287.04 J kg^{-1} $°K^{-1}$ is the gas constant for dry air; $q_s = 0.622e_{sat}/(P - (1 - 0.622)e_{sat})$ with units kg/kg; and saturation vapor pressure $e_{sat} = e_s f_w$ where $\log_{10} e_s = (0.7859 + 0.03477T_{air})/(1 + 0.00412T_{air})$ is the ideal saturated vapor pressure in 0.1 kPa and $f_w = 1 + 10^{-6}P(4.5 + 0.0006T_{air}^2)$ is a correction term (Gill 1982). We used these equations with the monthly data as well as the other meteorological data sets.

To estimate the surface energy budget for offshore waters, we increased inshore measurements of wind speeds by 50%, increased inshore measurements of air temperatures at 09:00 h by 1°C and decreased them by 1°C at 15:00 h, and decreased inshore measurements of relative humidity by 5% in the morning and increased them by 5% in the afternoon. These assumptions are based on a comparison of inshore and offshore meteorology (Fig. 3) and are within the observed range of these variables. Offshore winds were 28–125% higher, offshore air temperatures ranged from

Table 2. Comparison of temperature changes computed from net heat fluxes estimated from NCEP reanalysis I data with within-lake temperature changes computed from area weighted mean temperatures for the full water column based on temperature data from the northern offshore site. Temperatures are assumed uniform lakewide. The slight differences between the averaging periods for the reanalysis data and lake data occur because cooling begins with the intensification of winds in May and our sampling program began in June 1994. GG1, GG2, and GG3, Gaussian grid points 1, 2, and 3.

Reanalysis I	15 May 1994–01 Sep 1994 (°C)	01 Sep 1994–01 May 1995 (°C)	15 Jul 1994–15 Jul 1995 (°C)	15 May 1994–15 Jun 1994 (°C)
GG1 (western basin)	−0.01	+1.0	+1.55	−0.54
GG3 (eastern basin)	−1.25	+1.7	+1.32	
GG2 (southwestern basin)	−2.8	+3.8	+1.6	
Global 1 (northern basin*)	−0.9	−3.6	−4.8	−0.5, −0.14†
Average GG1 and GG3	−0.6	+1.35	+1.4	
Net change lake	−0.7†	+1.3	+0.6	

* solar from GG1;
† 01 Jun 94–01 Aug 1994.

1°C warmer in the morning to 2–3°C cooler in the afternoon, and relative humidity offshore was 0–10% lower in the morning and 5–18% higher in the afternoon. Although our interpretation could be confounded by year-to-year variability, the pattern of more muted air temperature and relative humidity and higher winds offshore is to be expected. The land-based meteorological data were too intermittent for the period 1994–1996 to assess between-year variability, but NCEP reanalysis 1 and ERA-I data show wind speeds and air temperatures were similar during the periods of between-year comparisons, except that winds were higher in January 1996 than in the previous year (Fig. 4; ERA-I data not shown). Verburg and Hecky's (2003) observations of winds being 50% higher at a buoy station than on land during the rainy season extends our strategy for computing winds to the rainy season.

We calculate fluxes for the northern basin using water temperatures from 10 m depth at 09:00 h (J. F. Talling pers. comm.) from Fish's (1957) and Talling's (1966) time-series measurements, which are from the same time period as the monthly meteorological data. Using temperatures from 10 m avoids any confounding influence of diurnal heating. We

Table 3. Comparison of temperature changes as in Table 2 but using ERA-I reanalysis data. Grid points were selected and averaging performed to allow comparisons with the results in Table 2. ERA-I grid points 1 and 2 are intermediate between reanalysis I global grid point 1, and ERA-I grid point 10 is located similarly to Gaussian grid point 2. The western basin averages were done using ERA-I grid points 1, 4, 7, and 10 and the eastern basin averages were done using ERA-I grid points 3, 6, 9, and 12. The northern (southern) averages were for the six northernmost (southernmost) grid points.

ERA-I	15 May 1994–1 Sep 1994 (°C)	1 Sep 1994–1 May 1995 (°C)	15 Jul 1994–15 Jul 1995 (°C)	15 May 1994–15 Jun 1994 (°C)
Western basin	−0.4	+0.5	+0.2	−0.11
	−0.2*	+0.8*	+0.6*	−0.07*
Eastern basin	−0.2	+0.7	+0.6	−0.09
	−0.1 *	+0.9*	+1.0*	−0.06*
Southwestern basin, grid point 10	−0.9	+0.2	−0.7	−0.2
	−0.7*	+0.6*	+0.3*	−0.14*
Northern offshore basin,				
Grid point 1	−0.1	+0.6	+0.5	−0.07
				−0.1†
Grid point 2	+0.05	+0.8	+1.0	−0.03
				−0.04†
Average eastern and western	−0.3	+0.6	+0.4	
	−0.2*	+0.8*	+0.8*	
Net change lake	−0.7†	+1.3	+0.6	

* Assumes temperatures in the southern half of the basin are 0.5°C colder than in the northern.
† 1 Jun 94–1 Aug 1994.

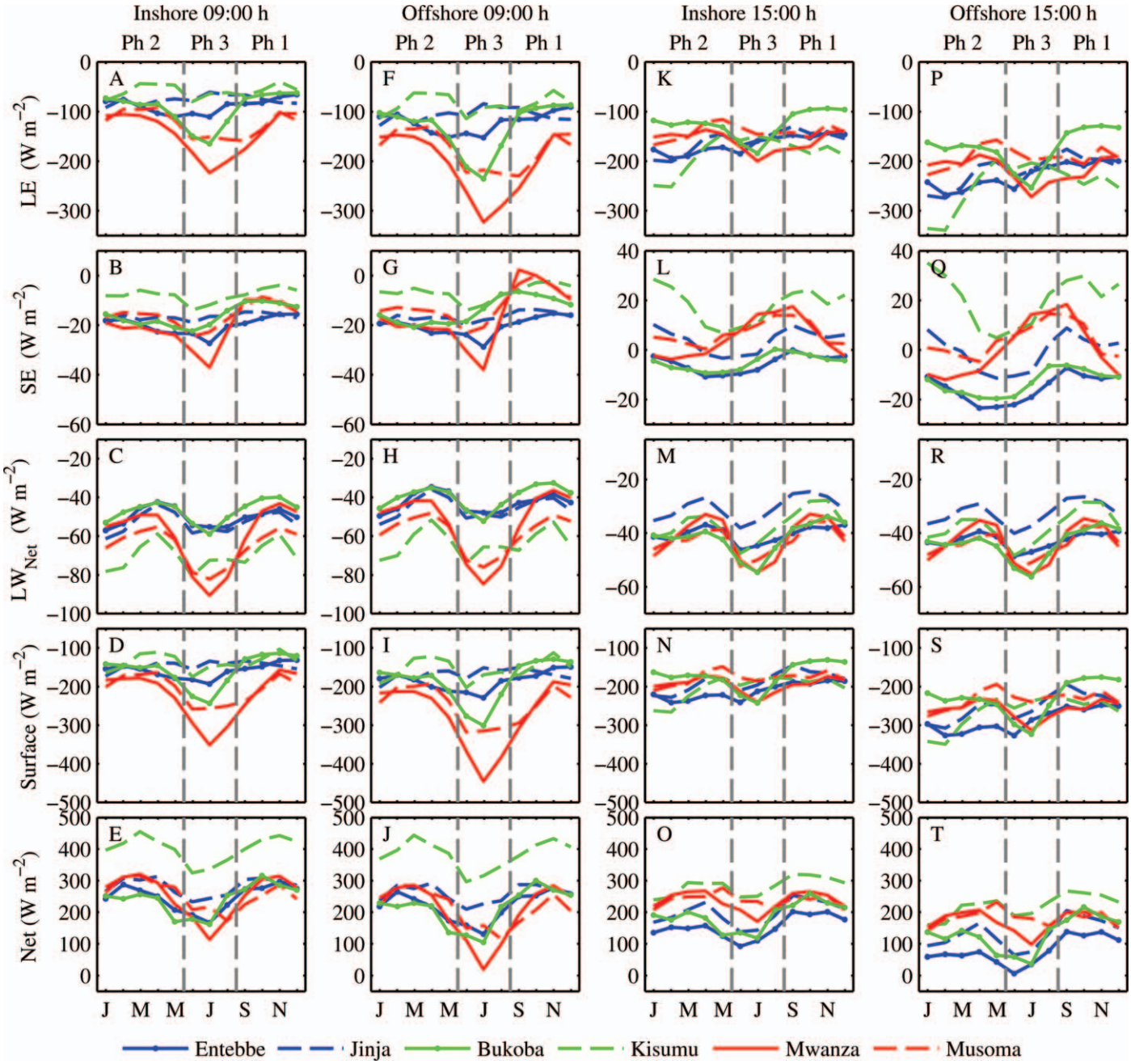

Fig. 5. Monthly estimates for the six inshore stations (Figs. 1, 2) and nearby offshore sites of latent and sensible heat fluxes, net longwave radiation (LW_{Net}), surface heat fluxes, and net heat fluxes at 09:00 h and 15:00 h. Abbreviations as in Fig. 3. Vertical dashed lines delineate phases.

averaged the temperatures by month, and, based on CTD profiles taken at several times of day intermittently during this study (data not shown), assumed surface-water temperatures at 15:00 h were 0.75°C warmer. Based on the analysis of Cozar et al. (2012), we subtracted 0.5°C in all months except January to obtain temperatures for the southern basin. We added 0.4°C to the offshore temperatures to obtain inshore temperatures to the north, and, in the absence of other data, assumed the same applies to other inshore locations. These offsets were determined based on our synoptic surveys and inshore–offshore transects (Table 1). Results are in Fig. 5.

Calculated fluxes are sensitive to surface-water temperatures. Decreasing surface temperatures 0.5°C relative to those measured at the northern offshore stations caused calculated latent and surface heat fluxes to be ~ 15 and ~ 25 W m^{-2} less negative, respectively. For temperatures at northern stations 1.2°C warmer than southern, calculated surface heat fluxes are equivalent at Entebbe and Mwanza in January and February (data not shown). With monthly north to south temperature differences varying by at most 1.2°C (Cozar et al. 2012), the between-station estimates of latent and surface heat fluxes have uncertainty of 40 and

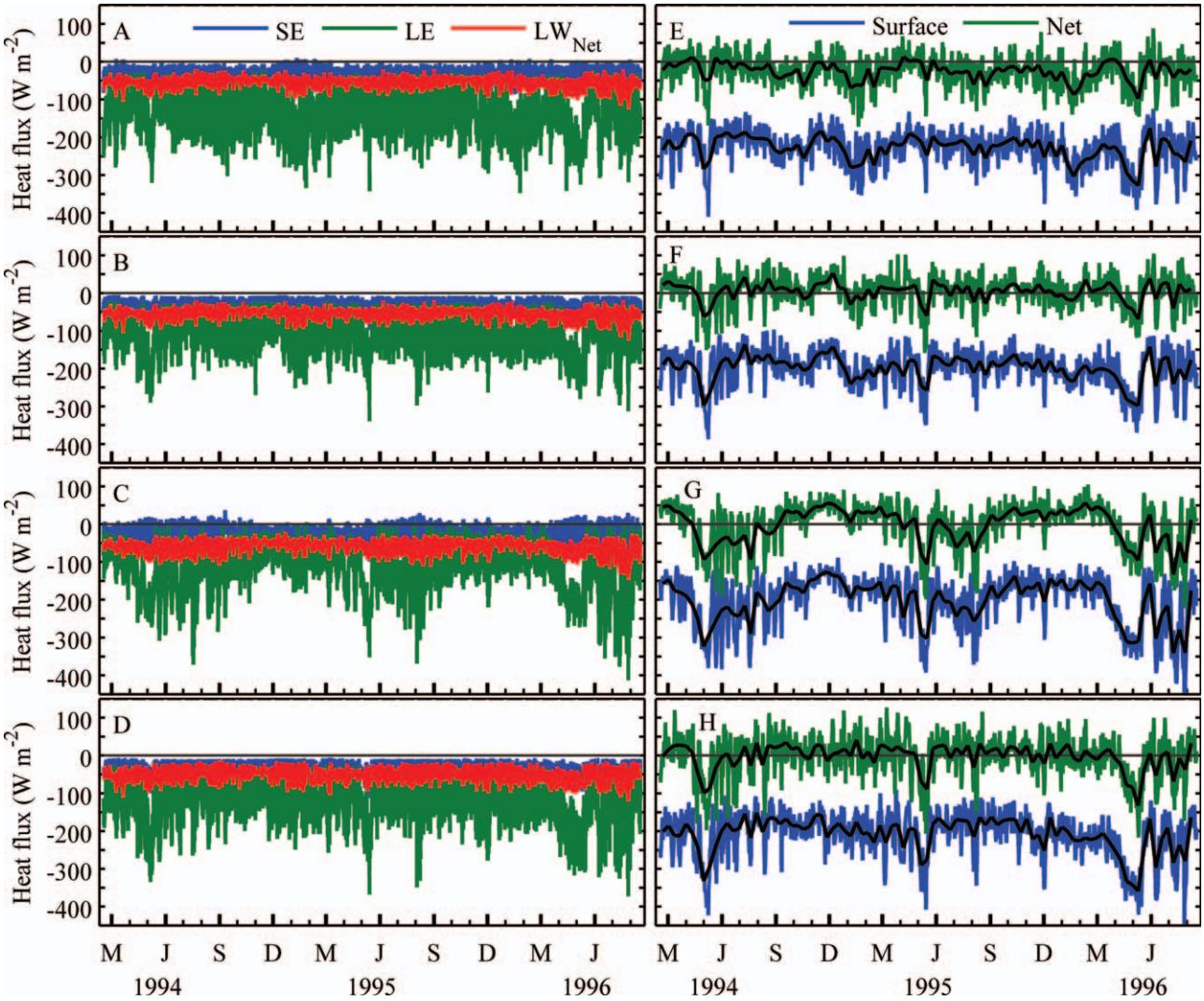

Fig. 6. (Left panels) Time series of 6 hourly sensible and latent heat fluxes and 6 h average net longwave radiation, and (right panels) daily averaged and 10 d averaged (black line) surface and net heat fluxes from NCEP reanalysis 1 data from March 1994 through August 1996 averaged over the (A, E) northern sector, global grid point 1; (B, F) mid-lake western sector, Gaussian grid point 1; (C, G) mid-lake eastern sector, Gaussian grid point 3; and (D, H) southwest sector, Gaussian grid point 2. Tick marks are midmonth.

60 W m^{-2}, and the uncertainty in sensible heat fluxes and net longwave radiation is of order $\sim$ 10 W m^{-2}.

Calculations: Inshore and offshore comparisons with measured data—Using the 30 min averaged data in the northern archipelago obtained in 1994–1996, we estimated the diel inshore and offshore surface heat fluxes for 2 week periods during the northeast and southeast monsoons. Surface-water temperatures are based on our diel measurements inshore in June and our inshore–offshore transects, which indicated temperatures were 0.6–0.8°C warmer inshore near the start of the southeast monsoon (sampling regime described in Table 1). For June in offshore (inshore) waters, the minimum surface-water temperature was 24.8°C (25.4°C) and occurred at 07:00 h, the maximum was 25.8°C (26.6°C) and occurred at 14:00 h, and, based on rates of change of temperature overnight, temperatures were assumed to be 25.2°C (26°C) at midnight. For January, based on our monthly measurements in northern offshore waters, temperatures were assumed to be 0.6°C warmer offshore than in June, and, from our inshore–offshore transects, 0.6–0.8°C warmer inshore. We assumed a similar pattern of diel change in January as in June. Thus, in offshore (inshore) waters, the minimum surface-water temperature was 25.4°C (26°C) and occurred at 07:00 h, the maximum was 26.4°C (27.2°C) and occurred at 14:00 h, and temperatures were 25.8°C (26.4°C) at midnight. We used an average value of net longwave radiation of -50 W m^{-2} (MacIntyre et al. 2002; NCEP reanalysis 1 data, Fig. 6; ERA-I reanalysis, not shown) and set atmospheric pressure equal to 88.5 kPa (Fig. 2).

Calculations: NCEP reanalysis data—The NCEP reanalysis data are available for 03:00 h, 09:00 h, 15:00 h, and 21:00 h local time. The global grids are 2.5° by 2.5° and the

Gaussian grids are approximately 1.9° by 1.9°. The reporting conventions differ based on the spatial averaging convention. For the Gaussian grid points, wind speed and direction, air temperature, and relative humidity are given for 6 h after the reported time, and shortwave and net longwave radiation are averages presented for the 6 h beginning at the reported times (http://www.esrl.noaa.gov/psd/data/gridded/data.ncep.reanalysis.surfaceflux.html). For the global grid point, near Entebbe, data are instantaneous values for the reported time and net shortwave and net longwave data are not available (http://www.esrl.noaa.gov/psd/data/gridded/data.ncep.reanalysis.surface.html). We corrected for these offsets and present results for the reported times. Our estimates of net heat fluxes are based on summing our calculated latent and sensible heat fluxes for the four times of day and the 6 h average net shortwave and net longwave radiation data reported for the four times each day for March 1994 through August 1996. We used the net shortwave and net longwave radiation from Gaussian grid point 1, north of Bukoba, in our estimates of net heat fluxes for global grid point 1 because of the larger spatial overlap than with Gaussian grid point 3. Comparisons of 5 d averaged net shortwave and longwave radiation from the two sites indicated both were similar, with occasional differences of 10–20 W m^{-2}. Calculations of surface and net heat fluxes at global grid point 1 using averaged net shortwave and longwave radiation from the two Gaussian grid points was thus of the same magnitude as when only the one grid point was used. Calculations of latent and sensible heat fluxes use water temperatures from 10 m depth from the CTD profiles in 1994–1996 interpolated from our monthly and bimonthly measurements with the 10 m data used to avoid the confounding influence of diurnal heating. Water temperatures are not corrected for time of day or location on the lake. We also computed fluxes assuming surface temperatures were 0.5°C warmer or colder and find that the surface and net heat fluxes are ~ 25 W m^{-2} more or less negative. These results are similar to those obtained in our sensitivity analysis using the monthly averaged data.

Comparisons of the reanalysis I and II data with the monthly averaged meteorological data from 1994–1996 showed that reanalysis I data underestimate wind speeds whereas reanalysis II gives values more similar to measurements. Reanalysis I wind speeds increase in mid-May with a tendency for lower values during June, July, and August except in La Niña years, whereas wind speeds modeled with reanalysis II intensify in May and are higher than reanalysis I estimates in the following 3 months (data not shown). Both reanalysis products underestimate air temperatures. Comparison of the temperature change computed from the surface energy budgets (*see* Calculations) and the integrated lake temperatures at the northern offshore station showed that surface energy budgets from reanalysis I data quantified the temperature changes over cooling and warming periods with reasonable accuracy (Table 2), whereas the predicted heating and cooling were several degrees too high or too low with reanalysis II data. Hence, we use reanalysis I data in our analysis.

Calculations: ECMWF ERA-I reanalysis data—The grid resolution is finer with ERA-I data than for NCEP data, with grid points 0.75° apart. Surface data are 6 h averages and radiation data are 12 h averages. With respect to the southeast monsoon, winds begin to intensify in May and maximal winds occur in July and August. This pattern differs from that in reanalysis I, where greater intensification begins in May, and that observed in measured data near Mwanza (data not shown). Calculations were performed as for NCEP reanalysis I data in which we used air temperature, relative humidity, and wind speed from the reanalysis data and our monthly temperature measurements from 10 m depth to compute latent and sensible heat fluxes for the four times of day. As for NCEP reanalysis 1 data, we performed our analysis assuming temperatures were similar over the lake, and, following Cozar et al. (2012), assuming temperatures in the southern half of the basin were 0.5°C cooler than those we had measured to the north. Net longwave data from ERA-I grid point 1 was only 9 W m^{-2} more negative than net longwave calculated from ERA-I downwelling thermal radiation and longwave computed from water temperatures from 10 m depth at the northern offshore station. Given the good accuracy and lack of temperature measurements at other locations on the lake, we used the net longwave product in computations for all grid points. Similar to results with NCEP reanalysis 1 data, the surface energy budget computed from ERA-I data gave reasonable estimates of temperature changes relative to areal weighted measurements in the lake, except that it underestimated the temperature decreases in the southeast monsoon and the subsequent heating (Table 3). For this reason, we show results with NCEP reanalysis I data and provide additional context with the ERA-I results.

Calculations: Turbulence parameters—We computed the coefficient of eddy diffusivity K_z within the upper mixed layer following Tennekes and Lumley (1972) as $K_z = cul$ where u and l are turbulent velocity and length scales. We let l be mixing-layer depth or overturning length scale, computed u following Taylor (1935) as $u = (\varepsilon l)^{1/3}$ where ε is integrated rate of dissipation of turbulent kinetic energy computed from the flux of turbulent kinetic energy into the mixed layer (F_q), and the coefficient $c = 0.7$ was based on unpublished intercomparisons of calculations from field data with model results in Rueda and MacIntyre (2010). Following Imberger (1985), $F_q = 0.5\ (w_*^3 + C_N^3 u_{*w}^3)$ and $\varepsilon = 0.82\ F_q/l$ where $w_* = (\beta l)^{1/3}$ is the turbulent velocity scale for thermals; $u_{*w} = (\rho_a C_d U^2/\rho_w)^{1/2}$ is the turbulent velocity scale for wind where U is wind speed, ρ_a and ρ_w are air and water density respectively, and the drag coefficient C_d has been corrected for atmospheric stability and instrument height; the neutral drag coefficient $C_N = 1.33 \times 10^{-3}$; and buoyancy flux $\beta = g\alpha H/\rho c_p$, where g is gravity, α is coefficient of thermal expansion, H is net heat flux, ρ is density, and c_p is thermal heat capacity. Within the more stratified part of the water column, we computed K_z following Osborn (1980): $K_z = \Gamma \varepsilon N^{-2}$, where Γ is a mixing efficiency with maximal value 0.2, ε is rate of dissipation of turbulent kinetic energy, and N is the buoyancy frequency in radians per second.

Results

Seasonal and large-scale variations in meteorology—East–west differences in evaporation and precipitation around the lake are pronounced because the prevailing southeasterly winds over Lake Victoria are dry after traversing the East African land mass, whereas rainfall is higher to the west (Fig. 1). In consequence, annual evaporation is greater along the lake's eastern perimeter (1.8–2.3 m yr^{-1}; Mwanza, Musoma, and Kisumu) than along the western margin (1.2–1.8 m yr^{-1}). Annual rainfall is highest along the western margin (Bukoba, 2.2 m yr^{-1}) and lowest in the southeast (Musoma and Mwanza, 0.9–1.2 m yr^{-1}). With the exception of Bukoba, evaporation was greater than rainfall at all of the shoreline stations. Similar to other studies (Krishnamurthy and Ibrahim 1973; Kite 1981), rainfall and evaporation dominated the lake's water budget during our study period, with increased rainfall causing the lake level to rise by 20–40 cm and increased discharge through the Nile in May, June, and July, following the long rainy season (data not shown).

As a result of the greater cloud cover to the west, solar radiation and air temperatures were lower and relative humidity higher at the three western (Bukoba, Entebbe, and Jinja) as opposed to eastern (Kisumu, Musoma, and Mwanza) meteorological stations (Fig. 2A,I,J,M,N). Seasonal variability in solar radiation is muted but peaks occur at the equinoxes (March, September) and minima at the solstices (June, December); the two rainy seasons, with their higher cloud cover, are centered on April and November (Fig. 2A,B). Atmospheric pressure increased in April–May coincident with peak rainfall and, at most stations, coincident with the onset of higher winds, and plateaued during the southeast monsoon (Fig. 2C) with its typically cooler air temperatures except to the south in the afternoon (Fig. 2M,N), lower relative humidity at the more southerly stations (Fig. 2O,P), and higher morning wind speeds, particularly to the south and west (Fig. 2G). These monthly average data quantify the spatial–temporal variability in meteorological forcing due to the movement of the different air masses that flow over the lake and the lake effect itself.

Strong diel signals occur in wind speed and direction, air temperature, and relative humidity and are modulated by seasonality (Fig. 2). The land breeze predominates from early evening to midday, when air temperatures over land are cooler than those over the lake, and the stronger lake breeze develops in the afternoon (Figs. 1, 2G,H). The land–lake breeze dynamic creates spatially variable changes in wind direction (Figs. 1, 2K,L). The land breeze increases during the long rains except to the north and, particularly at the more southerly stations, tends to remain high during the southeast monsoon. Controls on the lake breeze are more complex. For example, it was high at Entebbe during phase 2 and began to taper during the monsoon (phase 3). It peaked mid-monsoon at Bukoba and later in the monsoon at Mwanza and Musoma. Morning air temperatures were at least 2°C cooler than afternoon temperatures, and relative humidity was greater in the morning than in the afternoon (Fig. 2M–P). The southeast monsoon influences meteorology over the entire lake, but the changes were not spatially consistent. Air temperatures decreased in the morning and afternoon at most stations. Decreases in cloud cover and relative humidity and increases in wind speed were larger to the south and west. Given these patterns, water temperatures in the southern and western regions of the lake will cool more in response to the southeast monsoon, and given the greater increases in wind speed and decreases in relative humidity during morning land breeze conditions, cooling of the lake will be larger at night and in the morning.

Diel meteorology at inshore and offshore sites—Land–lake breeze conditions dominated the period of record, with flows from land to lake in the morning and the converse in the afternoon. The diel ranges of air temperatures (Fig. 3A,B) and relative humidity (Fig. 3C,D) were larger inshore than offshore. Wind speeds were higher and persisted for longer periods of time offshore (Fig. 3 E,F). In January and in June, wind speeds offshore increased with the onset of the lake breeze and tapered during the afternoon with low winds at night. Lake breeze conditions persisted longer offshore in June (Fig. 3 G,H). In December 1994 (not shown), the influence of the northeast monsoon was apparent at the offshore site as winds remained northerly over several diel cycles. Because of the combination of higher and more sustained winds offshore, latent heat fluxes were greater offshore than inshore (Fig. 3 K,L). Nighttime values during low winds were typically -50 W m^{-2} and daytime values in the range -100 to -150 W m^{-2}. However, when winds were elevated 11–13 January 1995, latent heat fluxes at night offshore reached -250 W m^{-2}. Sensible heat fluxes were always low (Fig. 3 M,N).

Surface heat fluxes, the sum of latent and sensible heat fluxes and net longwave radiation, were often two times higher offshore than inshore during the day (Fig. 3O,P). Surface heat fluxes at night were ca. -100 W m^{-2} but slightly larger offshore and reached -300 W m^{-2} during windy periods. Seven periods with elevated winds occurred in the 2-month period when the meteorological station was at the FTI offshore of Entebbe in December 1994–February 1995. When averaged over a month, the surface heat fluxes also indicate greater cooling offshore (January 1995 offshore, -170 W m^{-2}; January 1996 inshore, -121 W m^{-2}; June 1994 offshore, -152 W m^{-2}; June 1995 inshore, -116 W m^{-2}). Because winds, and hence latent heat fluxes, tend to be highest in the day both inshore and offshore, the net heat flux into the lake is reduced relative to incoming shortwave radiation (Fig. 3I,J,Q,R). Because winds are higher offshore, more of the incoming heat will be mixed downwards, causing a deeper mixed layer and cooler temperatures offshore than onshore. This effect is increased by the longer duration of higher winds offshore and resulting longer periods of cooling relative to heating. Thus, warmer water temperatures and shallower mixed layers are anticipated in the northern inshore waters relative to those offshore.

Lakewide surface energy budgets—The east–west variability in meteorological forcing induced spatial variability

in heat fluxes, with the differences typically more evident at 09:00 h. Latent heat fluxes and net longwave radiation were greater on the eastern side of the basin because of the low humidity, lower cloud cover, and generally higher winds (Fig. 5 A,C,F,H). Sensible heat fluxes tended to be positive on the eastern side of the lake in the afternoon with its warmer air temperatures from May through September (Figs. 2N, 5L,Q). The southeast monsoon induced spatial variability from north to south. Because of the increased winds and lower relative humidity particularly to the south, latent heat fluxes increased at Bukoba, Musoma, and Mwanza, with monthly average 09:00 h values at Mwanza in excess of -300 W m^{-2} (Fig. 5A,F). Latent heat fluxes made the strongest contribution to inshore–offshore differences in heat fluxes. Monthly average latent heat fluxes are 20–50% larger offshore than onshore, with the difference increasing as fluxes increase.

The surface heat fluxes showed a stronger north to south difference than east to west, with the pattern more evident in the morning (Fig. 5D,I,N,S). Surface heat fluxes remained relatively constant over the year at the northern stations but became increasingly more negative during the southeast monsoon at the southern and eastern stations and at Bukoba to the west. Variability in surface heat fluxes in the afternoon was muted, but losses were accentuated at Mwanza and Bukoba during the southeast monsoon and at the northern stations (Entebbe, Jinja, and Kisumu) during January and February. Greater surface heat losses during land breeze conditions occurred to the south than the north during the southeast monsoon.

Net heat fluxes apply to daytime conditions (Fig. 5 E,J,O,T). Because of the absence of nighttime data, the surface heat flux at 09:00 h, representative of land breeze conditions, provides an estimate of net heat flux at night. The increased solar radiation during the equinoxes contributed to seasonality in net heat fluxes at 09:00 h and 15:00 at all stations. Net heat gains were largest during phases 1 and 2, at the time of the temperature increases in the lake described in Talling (1966). During phase 2, the net heat fluxes were largest in March and April, when rainfall tends to increase and peak (Fig. 2B). During the afternoon, the east–west pattern reemerged from January through August, with greater net heating in the day at the eastern stations.

In summary, the largest spatial variability in the surface energy budget was induced by the southeast monsoon, which caused greater heat losses to the south during land breeze conditions and more muted heat gains in the day, and by the east–west differences in cloud cover, which led to higher latent heat losses during land breeze conditions and greater diurnal heat increases to the east during the long rains and southeast monsoon. Surface heat fluxes were less negative inshore than off, allowing for greater water temperature decreases at night offshore, and net heat fluxes were greater inshore. This pattern will lead to warmer lake waters at northerly stations inshore. The seasonal differences in heating and cooling create the annual cycle of stratification and the spatial differences create temperature differences between inshore and offshore waters and across the main basin.

The calculated fluxes in Fig. 5 provide an assessment of climatic and lake-induced controls on spatial variability in the surface energy budget. The magnitude of the fluxes admittedly has a certain degree of error associated with the approximations required to estimate offshore meteorology. For example, increasing offshore winds by 200% and air temperatures by 0.5°C at 09:00 h causes computed latent, surface, and net heat fluxes to become 50–100 W m^{-2} more negative. The largest decreases occur at the more southerly stations during the southeast monsoon and would induce net heat loss. The following analysis of temporal and spatial patterns provides another approach to assess the accuracy of the estimated fluxes.

Interannual variability in meteorological forcing—The climatology of East Africa is strongly influenced by El Niño–Southern Oscillation (ENSO) cycles and the Indian Ocean Dipole (Nicholson 1996; Clark et al. 2003). The patterns described in Figs. 2 and 5 average over multiple ENSO cycles and the onset of warming in the Indian Ocean. Our 1994–1996 study was conducted during a period with near-constant temperatures in the Indian Ocean, a weak El Niño during 1995 (Niño 3.4 Region = +1), a positive anomaly of the Indian Ocean Dipole during 1995, and a weak La Niña in 1996 (Niño 3.4 Region = -1; http://www.cpc.ncep.noaa.gov/data/indices/). Comparison of the meteorological data and the NCEP reanalysis I data for the period 1958–1969 with that for 1994–1996 indicates that wind speeds during the long rains were similar but winds were 50% higher at some stations during the southeast monsoon in the earlier period. In the following, we contrast meteorological conditions during our experiment on a north to south transect using data from global grid point 1, Gaussian grid point 1, and Gaussian grid point 2 (Figs. 1A, 4).

The 5 d averaged NCEP reanalysis 1 data further differentiate the north to south patterns seen in the monthly averaged data and differentiate patterns related to ENSO cycles (Fig. 4). The clearest seasonal signals are seen to the south (Fig. 4M–R). Beginning in May, when air pressure rose as the ITCZ began to move north (Fig. 2), solar insolation decreased, daytime air temperatures and winds increased, and relatively humidity decreased. The largest changes occurred in 1996, the La Niña year. In June, conditions became more variable in all years, with the large changes in solar radiation and wind speed suggesting the southeast monsoon is marked by frontal activity. Winds were low to the south from September through March. The northern (Fig. 4A–F) and mid-lake (Fig. 4G–L) sectors showed a similar pattern with respect to increased winds in May, but air temperatures and relative humidity were out of phase with warmer, less humid afternoons from December through June. Nocturnal, primarily northerly winds increased to the north beginning in the southeast monsoon and persisted until November. Increases in nocturnal, northerly winds also occurred mid-basin to the west and south, but the winds were weaker and the increases occurred progressively later to the south. Winds were least to the north and mid-basin to the west in December, but increased again in January or February, with the onset delayed at the mid-basin location. The different timing of winds from north to south is also

evident in the monthly averaged data in Fig. 2, but the additional reanalysis data during nocturnal, land breeze conditions further highlights the influence of the north-south movement of the ITCZ.

Diel and seasonal variability in the surface meteorology are similar with the ERA-I data (not shown). The major differences are greater solar insolation during August and September, early morning air temperatures about 1°C warmer, and a slower intensification of winds with the transition to the southeast monsoon such that wind speeds are lower in May than from June to August.

To evaluate the accuracy of the surface energy budget computed with the reanalysis data, we computed changes in water temperature for the heating and cooling periods in the lake for a full year and compared the changes with those computed from areal weighted mean water column temperatures from our monthly sampling at the northern offshore station (Tables 2, 3). Temperature change was computed as $\Delta T = (NHF)(T_D)(SA)/(V\rho c_p)$ where NHF is mean net heat flux per day, T_D is number of days, SA is lake surface area, V is lake volume, ρ is density of water, and c_p is heat capacity. The comparisons assume that the magnitudes of temperature change that occur at the northern station are similar lakewide. The changes in estimated surface-water temperatures in the ERA-I product at grid points away from the lake margin were similar to the measured changes at the northern offshore station and support our assumption (data not shown). The accuracy of the reanalysis data appears to depend on the fraction of the lake covered by each grid point. Coverage is about 25% for NCEP reanalysis I global grid point near Entebbe and the Gaussian grid point 2 to the southwest. The calculated heating and cooling at these two grid points is larger than for Gaussian grid points 1 and 3, which cover over 50% of the western and eastern basins respectively. For the cooling and heating periods, the average temperature change for the full lake, obtained as the average temperature change for Gaussian grid points 1 and 3, differed from the measured change at the northern offshore station by 0.1°C and by less than 0.1°C respectively (Table 2). With the assumption of spatially uniform temperatures or temperatures 0.5°C cooler in the southern half of the basin, the ERA-I data underestimated the temperature change under cooling by 0.4°C and 0.5°C and under heating by 0.7°C and 0.5°C respectively (Table 3). The average annual temperature changes for the eastern and western basins were +1.4°C (NCEP) and +0.4°C or +0.8°C, assuming the southern half is cooler (ERA-I), whereas areal weighted mean lake temperatures increased by 0.6°C. Additionally, the estimated change in temperature during the high winds in May at global grid point and Gaussian grid point 1 was −0.5°C, slightly less than the measured change in temperatures to the north. In contrast, the temperature decrease in northern waters estimated from ERA-I was 0.1°C. This analysis indicates a good congruence between changes in temperature based on within-lake measurements and those estimated from the surface energy budget using both reanalysis products.

Despite the congruence between the calculations and measurements, some discrepancies occurred. In particular, net heat loss occurred in northern waters in reanalysis I data (global grid point 1 from September to May and for the full year). In contrast, the heat budget with ERA-I for northern waters indicates net heating from August into the rainy season beginning in October and November and again from January through May, similar to results with NCEP reanalysis 1 data at Gaussian grid points 1 and 2. ERA-I appears to underestimate cooling during the southeast monsoon, although accuracy might improve by taking into account the effects of variable bathymetry. The differences in the seasonality and the magnitudes of wind speed, air temperature, and relative humidity in the two sets of modeled data are subtle. As discussed above, the most obvious differences are that air temperatures at 09:00 h are about 1° cooler and wind speeds intensify more in May in the NCEP product. These differences contribute towards our calculating more negative latent heat fluxes using NCEP reanalysis 1 data. The higher modeled shortwave radiation in the ERA-I product contributes to the tendency for net heating from September to May.

The overall good congruence between estimated and measured temperature changes provides confidence in describing fluxes with the two reanalysis products (Tables 2, 3). Because the goal of this paper is to illustrate dominant patterns, and these are similar with both products, and because NCEP reanalysis 1 data appear to more accurately capture net heat losses during the southeast monsoon, we illustrate results with that data set and present contrasts with ERA-I as appropriate.

Latent, surface, and net heat fluxes progressively became more negative from south to north at western grid points beginning at the end of the rainy season, and southerly regions remained negative for a longer period during the southeast monsoon (Fig. 6A,B,D,E,F,H). Net cooling was least in 1995, during El Niño conditions, and greatest in 1996, during La Niña conditions. The onset of net heating tended to occur a month or two earlier in northern waters, except during La Niña conditions, and transitioned to cooling in April or May (ERA-I, data not shown). Mid-basin to the east (Fig. 6C,G), NCEP reanalysis I data indicate latent heat fluxes were larger by -50 W m^{-2} during the windy period at the end of the long rains and during the intermittently windy periods of the southeast monsoon than at the same latitude to the west (Fig. 6B,F). In consequence, net cooling was greater to the east at those times, similar to calculations from the monthly data (Fig. 5). These results contrast with the ERA-I data, which show greater cooling to the west. The eastern sector of the lake showed weak net heating from September through early May (Fig. 6G). The positive net heat flux resulted from lower winds to the east, as the magnitudes of the other meteorological variables were similar during that period (data not shown). Our sensitivity analysis indicates that if surface-water temperatures were warmer to the east, the net heating computed for phases 1 and 2 would not persist. North to south trends computed using NCEP reanalysis I data would persist for surface-water temperatures 0.5°C lower to the south, as we computed with the ERA-I data. The larger and more persistent net heat losses to the south during the southeast monsoon agree with our monthly average data (Fig. 5), with monthly averages using time-

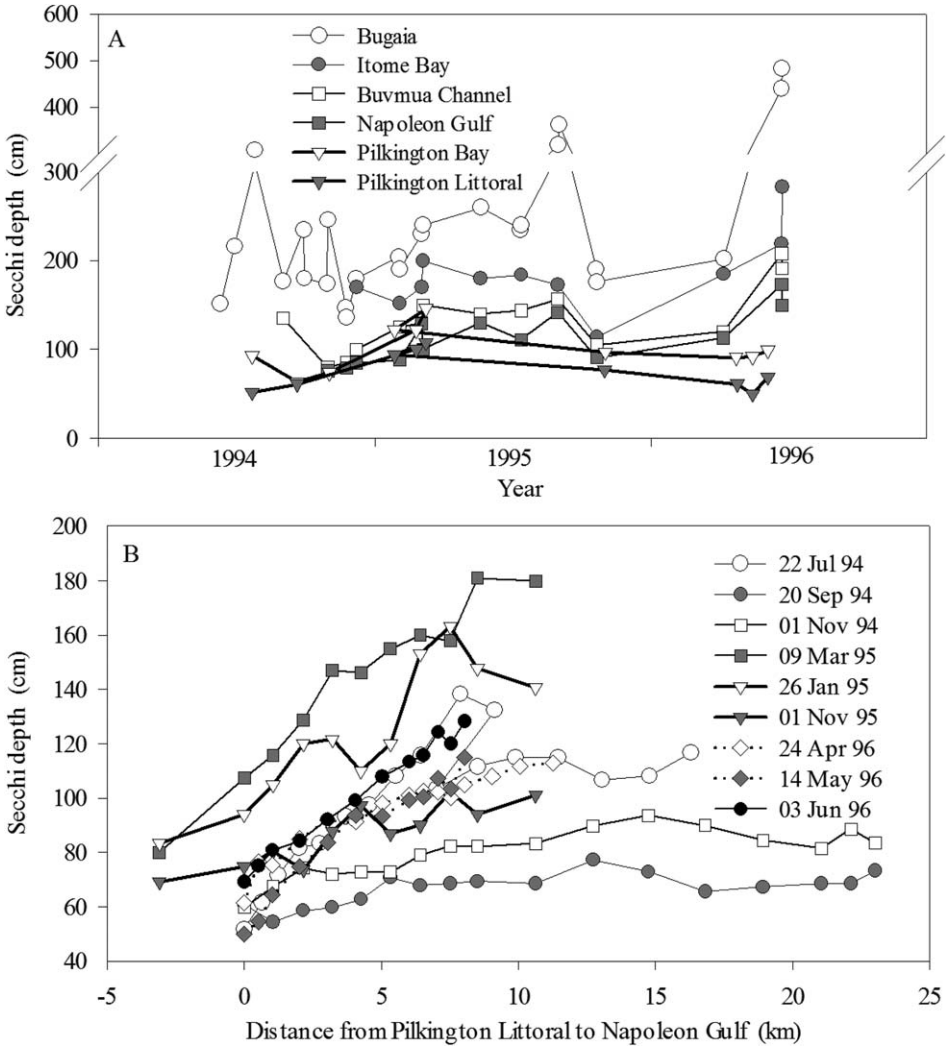

Fig. 7. (A) Secchi depths at five sampling stations in or near the northern archipelago and (B) Secchi depths obtained on transects from the littoral zone of Pilkington Bay to Napoleon Gulf from 1994–1996.

series data from the six meteorological stations for the period 1994–2003 (data not shown), and observations in Newell (1960) and Cozar et al. (2012).

Underwater light climate in the northern archipelago and northern offshore waters—The transparency of the water column varied over space and time. Secchi depths were always deeper offshore than inshore and were deepest during the southeast monsoon, and seasonal variability increased with distance offshore (Fig. 7A). The average Secchi depth at Bugaia station was 2.3 m (standard error [SE] = 0.8 m, $n = 25$), that at Napoleon Gulf was 1.1 m (SE = 0.3 m, $n = 13$), and that at mid–Pilkington Bay was 0.9 m (SE = 0.3 m, $n = 47$). Secchi depths also increased on transects from the littoral region in Pilkington Bay to Napoleon Gulf (Fig. 7B). Secchi depths were shallower and less variable along the transects during phase 1. The relation between the diffuse attenuation coefficient for PAR (k_d, m^{-1}) and Secchi depth (z_{Secchi}, m) is $k_d = 1.0\ z_{Secchi}^{-0.68}$ ($r^2 = 0.84$, $n = 43$) and was derived over a range of z_{secchi} of 0.7–7 m and k_d of 0.3–1.6 m^{-1}. On the basis of this relation, the attenuation coefficient for PAR at Bugaia station averaged 0.59 m^{-1} (SE = 0.12 m^{-1}). That in Pilkington Bay ranged from 1 to 1.6 m^{-1}. The larger k_d inshore will contribute to the greater warming of waters inshore.

Diurnal and seasonal stratification—Individual profiles illustrate the changing patterns of thermal stratification and depths of overturning over an annual cycle (Fig. 8). Our 08:10 h sampling in June 1996 captured inverse stratification in the full water column due to the large nocturnal heat losses at that time (Figs. 6E, 8A) and a diurnal thermocline in the upper 8 m at 11:15 h. The buoyancy frequency was less than 1 cycle per hour (cph), and the full water column overturned (Fig. 8B,C). Overturning below the diurnal thermocline was still evident in the profiles throughout the day (data not shown), indicating slow dissipation of the energy introduced at night. The temperature profiles from July, December, and

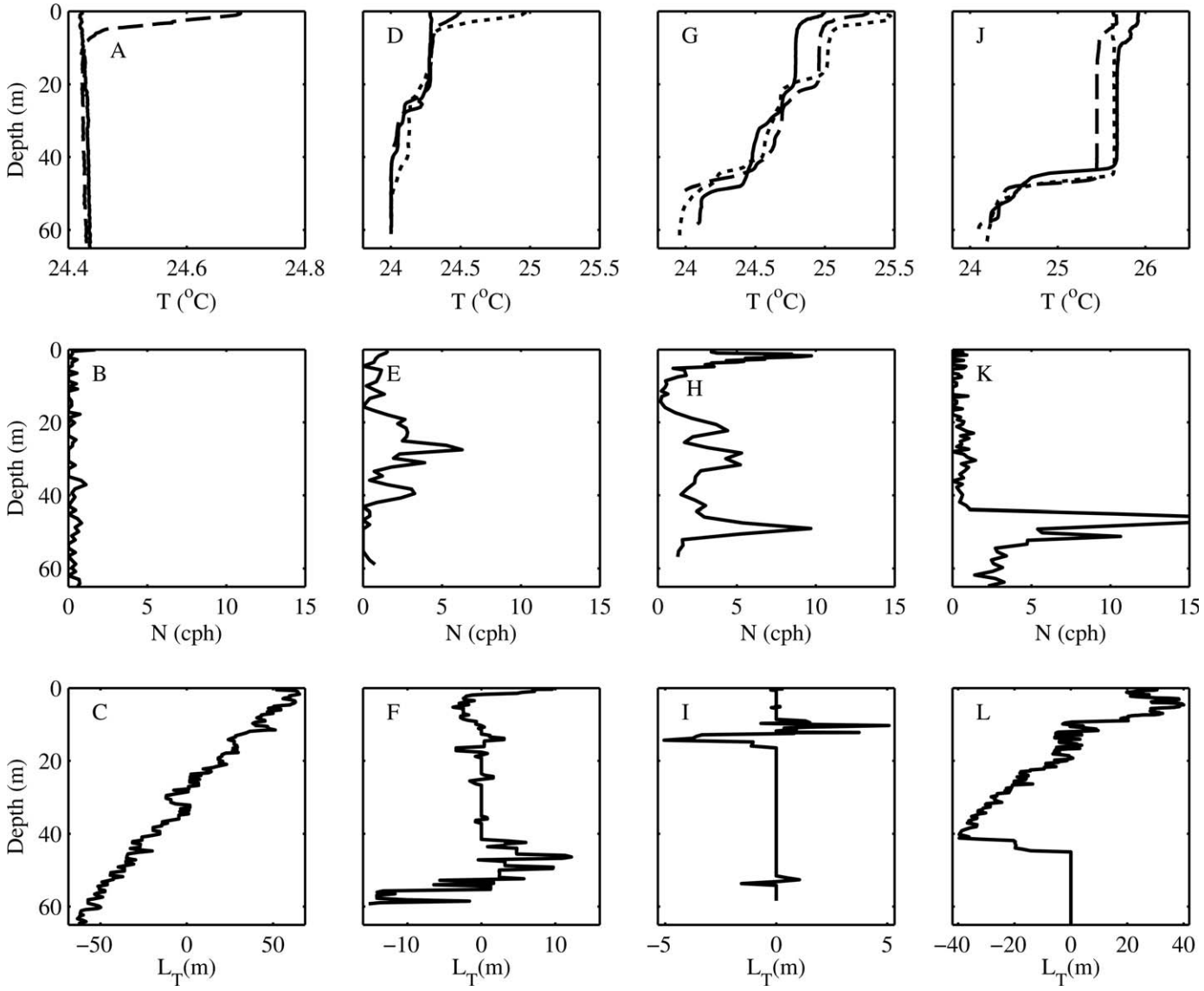

Fig. 8. (Upper panels) Temperature profiles, (middle panels) buoyancy frequency (N), and (lower panels) magnitude of overturning scales (L_T) for (A, B, C) 08:10 h and 11:15 h 22 June 1996; (D, E, F) 08:43 h, 10:37 h, and 12:16 h 27 July 1994; (G, H, I) 09:50 h, 11:14 h, and 11:55 h 07 December 1994; and (J, K, L) 15:22 h 03 March 1995, 13:54 h 04 March 1995, and 08:12 h 05 March 1995. Line type for profiles in panels A, D, G, and F is solid, long dash, and short dash for first, second, and third times given, respectively. Profiles of N and of overturns are for the earliest time on each sampling day or sampling sequence. Profiles were taken at the northern offshore station.

March illustrate the progressive development of stratification. Stratification was two-layered in July 1995 with the thermocline at 20 m and maximum buoyancy frequency of 5 cph (Fig. 8D,E). Overturns were intermittent and of order 1 m in vertical extent in the mid–water column but were 15 m in size near the bottom (Fig. 8F). Stratification was three-layered in December 1994 with associated subsurface peaks in buoyancy frequency near 25 and 50 m (Fig. 8G,H). The 5 m overturn in the upper, near isothermal layer would be residual from the previous night's cooling. Stratification was again two-layered in March with a deep mixed layer; the buoyancy frequency across the seasonal thermocline was 15 cph (Fig. 8J,K). Overturning from the previous night's cooling extended to 40 m, but no overturns were observed below the seasonal thermocline (Fig. 8L).

Diurnal thermoclines formed on each sampling day, but their depth was limited typically to 5 m. The mixed layer was deeper in the profiles from phase 2 than in those from phase 1 (Fig. 8). The variability in nocturnal winds indicates that within seasonal constraints, latent heat fluxes will vary from night to night, as will the depth of nocturnal mixing and water column temperatures (Figs. 4, 8J). Thermocline depths vary in the sequential profiles each day or over the course of a few days during the stratified period (Fig. 8D,G,J). Expansions and contractions of the thermocline by higher-order vertical internal wave modes can induce such variability (Newell 1960; MacIntyre et al.

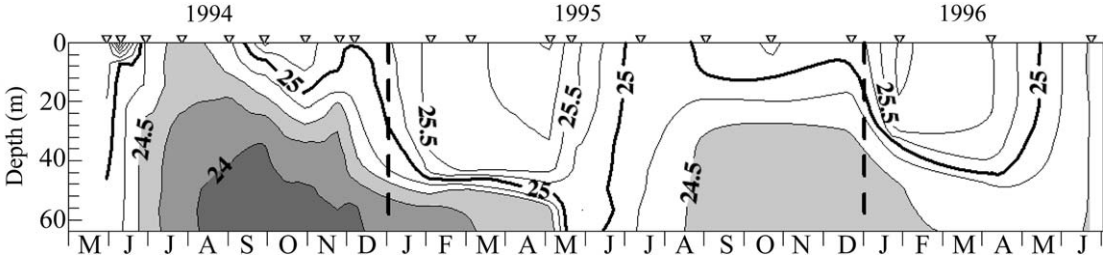

Fig. 9. Isotherms at the northern offshore stations during 1994–1996. Contours are 0.25°C. Inverted triangles indicate sampling dates.

2009; Vidal et al. 2013). Overturning in the upper water column was caused by heat loss (Fig. 8C,I,L), but that at deeper depths would have been caused by instabilities in the internal wave field or current shear (Fig. 8F).

By combining this information on the causes of mixing, magnitude of overturns, and heat fluxes and winds from the reanalysis data, we characterize the turbulence via estimates of the rate of dissipation of turbulent kinetic energy (ε), coefficient of eddy diffusivity (K_z), and time scales of mixing l/u, where l is overturning length scale and u is turbulent velocity. For heat losses of -350 W m^{-2} and winds $\sim$ 5 m s^{-1} as in June 1996 (Figs. 4A, 6E), calculated $\varepsilon = 9 \times 10^{-8}$ m^2 s^{-3} and $K_z = 0.7$ m^2 s^{-1}. For the deep overturning on 05 March 1995, heat losses were -250 W m^{-2}, wind speeds were 4 m s^{-1}, and mixing-layer depth was 40 m. Calculated $\varepsilon = 6 \times 10^{-8}$ m^2 s^{-3} and $K_z = 0.4$ m^2 s^{-1}. With the high surface heat fluxes, the contribution of β to turbulence production exceeded that for 4–5 m s^{-1} winds by one to two orders of magnitude. Values of K_z up to 0.05 m^2 s^{-1} computed for the mixed layer of Lake Baikal (Schmid et al. 2007), which would have lower buoyancy flux because of the cold water temperatures and hence lower latent heat fluxes, and values of order 10^{-2} m^2 s^{-1} and 10^{-3} m^2 s^{-1} as computed in oceanic diurnal thermoclines (Brainerd and Gregg 1993) support our estimate of such high values of K_z. For both cases, mixing time scales, $\tau_{mix} = l^2 K_z^{-1}$, indicate deep mixed layers, as in March 1995, and the full water column, as in June 1996, would turn over in just over an hour. The turbulent velocity scales of 0.02 and 0.01 m s^{-1}, far in excess of sinking or rising speeds of diatoms or cyanobacteria, and persistent overturning for several hours after sunrise despite the onset of diurnal stratification attest to the considerable mixing induced by nocturnal cooling.

To quantify K_z below the mixed layer (*see* Calculations: Turbulence parameters), we assumed $\varepsilon = 10^{-7}$ m^2 s^{-3}, as typically occurs in stratified flows with some internal wave activity (MacIntyre et al. 2009), N = 3 cph and 15 cph (Fig. 8), and obtained $K_z = 7 \times 10^{-4}$ m^2 s^{-1} and 3×10^{-5} m^2 s^{-1}. These values are upper bounds because of uncertainty in ε and use of a maximal value for Γ. The considerable overturning when the water column was weakly stratified in phase 1 supports K_z of order 10^{-4} m^2 s^{-1} with mixing likely by shear from internal waves or intrusions. During phase 2, typical values were likely lower than we calculate; enhanced mixing was occasionally mediated by nonlinear internal waves induced by strong winds, as will be discussed below.

Stratification of northern offshore waters—The seasonal pattern of stratification at the northern offshore station in this study (Fig. 9) was similar to that observed by Fish (1957) and Talling (1966). The lake gained heat in phases 1 and 2 and lost heat in phase 3, with the water column nearly isothermal early in the southeast monsoon. We did not capture isothermal events seen at the beginning of phase 2 by Fish (1957) and Talling (1966) with their more frequent profiling and attributed to high winds causing a deflection of the thermocline at the northern station. The depth of the 3 mg L^{-1} oxygen isopleth was coupled with the depth of the base of the thermocline from November through early May in 1994–1995 and in 1995–1996 (data not shown). The seasonal thermocline was eroded and hypoxia alleviated in 1995, coincident with the lakewide increased winds in late May of that year (Fig. 4D,J). As in the previous time-series data (Talling 1966), temperatures decreased in the lower water column in the latter half of the southeast monsoon (Fig. 9).

General patterns are explained by the meteorological data and computed fluxes (Figs. 2, 4–6). The higher solar radiation at the equinoxes contributed to the heating during phases 1 and 2 (Fig. 5). The increased northwesterly winds at night mixed the incoming heat downward and caused the deepening of the 25°C isotherm in September and October 1994 (Fig. 4; ERA-I data, not shown; Fig. 9). The 25°C isotherm shoaled in November and deepened again beginning in December. The formation of the seasonal thermocline by January was accompanied by increases in temperature (Fig. 9). Mixed-layer deepening could result from increased net heat losses, as computed using the NCEP reanalysis 1 data (Fig. 6). However, advection of warm water would be required to balance the heat budget. In contrast, the net heat fluxes computed with ERA-I data are positive. Consistent with net heating, and as will be discussed further below, the deepening of the mixed layer may be the result of the thermocline's being depressed by sustained westerly and later southerly winds throughout the day for much of phase 2 (Fig. 4F,L,R). As in the earlier studies, restratification at the end of the southeast monsoon was associated with cooling below 40 m. Area weighted mean temperatures of northern offshore waters decreased 0.7°C during the southeast monsoon in 1994, more than computed from the surface energy budgets for northern waters (Tables 2, 3), implying advection of cool water to northern offshore waters.

Lakewide transects—La Niña conditions prevailed in 1957 and El Niño conditions in 1958 (http://www.cpc.ncep.

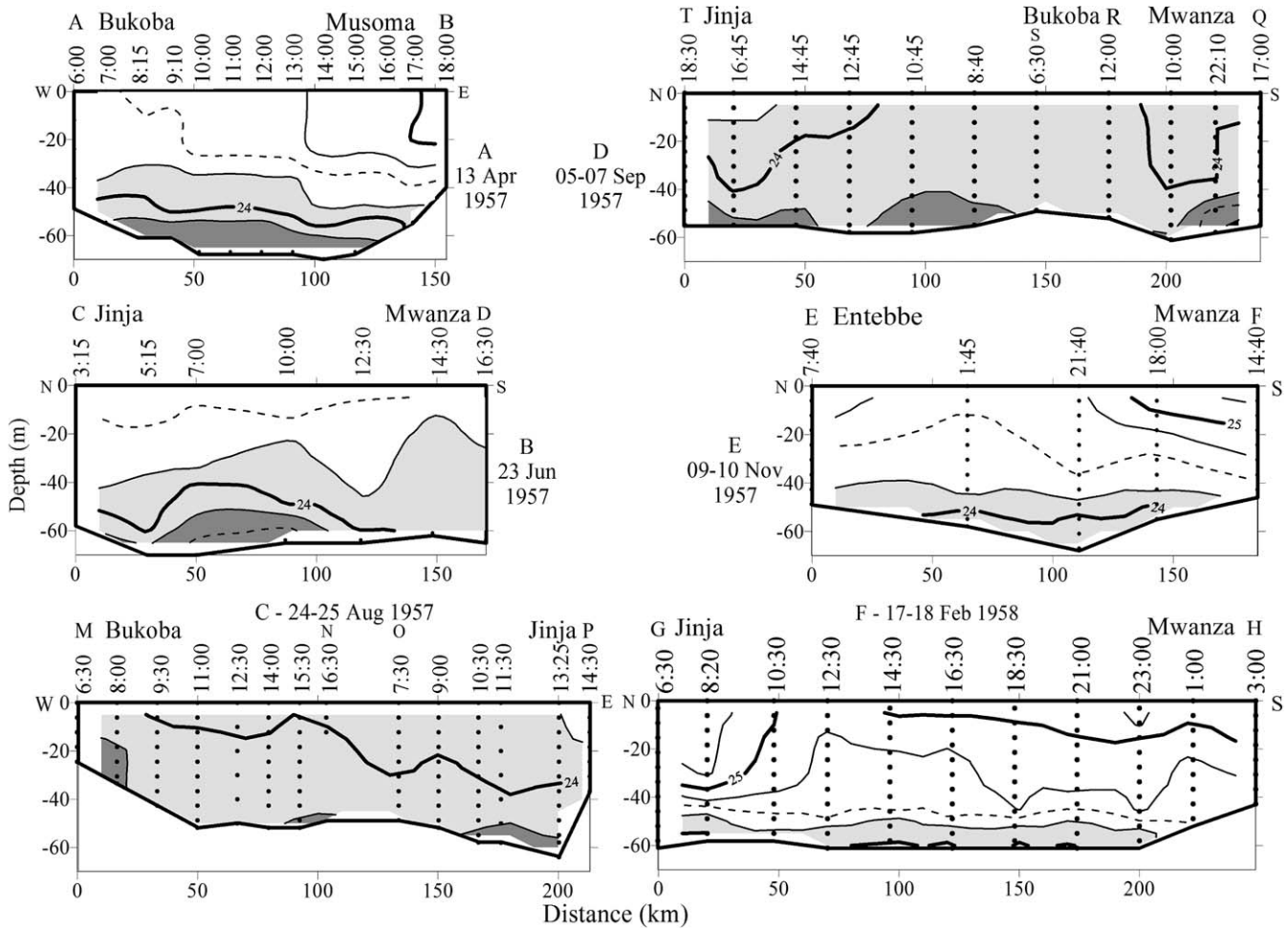

Fig. 10. Lakewide transects during 1957–1958 collected by Newell (1960) and reported by Talling (1966) as profiles, and reproduced here as isotherm plots. Locations of transects are in Fig. 1A and maintain Talling's (1966) original labeling. Contours are 0.25°C. (A) 13 April 1957; (B) 23 June 1957; (C) 24-25 August 1957; (D) 05-07 September 1957; (E) 09-10 November 1957; (F) 17-18 February 1958.

noaa.gov/data/indices/) when Newell (1960) conducted lakewide transects (Figs. 1A, 10). Winds during the long rains and southeast monsoon were elevated in 1957, similar to our study, although with more diel variability (NCEP reanalysis 1 data). On 13 April 1957, the deep waters show the seasonal stratification typical of phase 2, but the warmer waters near Musoma than Bukoba more likely result from the greater heating in April to the east than diurnal heating (Figs. 5, 6, 10A). Stratification, a lakewide thermocline tilt, and some doming of isotherms mid-lake were evident on the north to south transect 23 June 1957 during the southeast monsoon (Fig. 10B). The transect extended over the deepest region of the lake, and the coldest bottom waters were observed at those locations. The next transect, 24–25 August 1957, which was mid-basin and to the north, indicated cooler waters, a temperature difference of only 0.5°C at more offshore locations, and coolest bottom waters inshore near Bukoba and in the deeper profiles near Jinja (Fig. 10C). Water temperatures were similar in the north to south transect taken 2 weeks later, 05–07 September 1957, with coldest bottom-water temperatures when profiling was near the 60 m contour or in the most southerly waters (Fig. 10D). The lake had warmed considerably by 09–10 November, phase 1, with weak stratification below 40 m and the 24°C contour now at 50 m (Fig. 10E). The warmer southerly waters likely resulted from net heating to the southeast (Figs. 5T, 6G). Temperatures had increased further by 17–18 February 1958, phase 2, with 24°C water found only near 60 m. A thermocline was present in the lower 30 m offshore of Jinja, but stratification of the lower water column was weaker elsewhere (Fig. 10F).

In general, the seasonal cycle of heating and cooling described for the northern offshore waters (Fig. 9) applies to the lake as a whole (Fig. 10). Except during the southeast monsoon, temperatures to the east were warmer than those to the west, as expected from the net heating to the east from September through March (Fig. 6G). Lakewide cooling occurred during the southeast monsoon. The progressive warming thereafter and the deepening of the 24°C isotherm indicate that mixing occurred through the full water column. Residual cool water and stratification were found at the deepest depths sampled both at the beginning and end of the southeast monsoon. The coolest bottom-water temperatures in April 1957 were similar to those at the deepest depths during the southeast monsoon

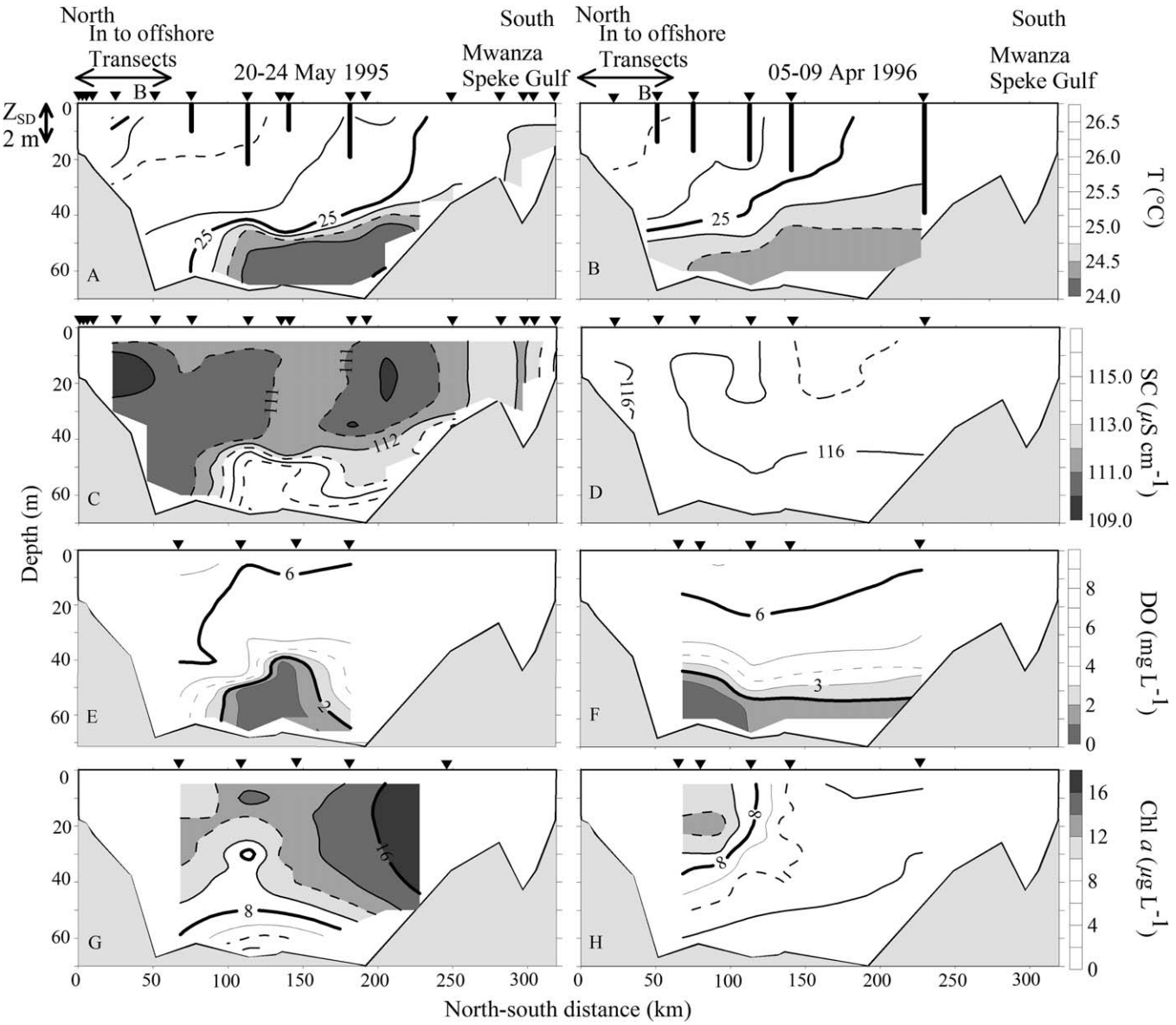

Fig. 11. (A, C, E, G) 20–24 May 1995 and (B, D, F, H) 05–09 April 1996 north (Jinja, Uganda) to south (Mwanza, Tanzania) transects across the main basin of Lake Victoria. (A, B) CTD temperature with Secchi depths denoted as bold bars from the surface with arrow to the left of (A) a scale bar indicating Secchi depth of 2 m; (C, D) CTD specific conductance at 25°C; (E, F) Hydrolab dissolved oxygen (DO); and (G, H) Chl *a*. *See* Fig. 1A for transect lines. Transect stations are indicated by arrowheads.

that year. Thus, it is not clear whether cooling due to the high winds at the end of the long rains and during the southeast monsoon resets the temperatures below 60 m each year.

The May 1995 cross-lake transect provides the first evidence that winds can induce lakewide up- and downwelling in Lake Victoria and concomitant reduced stratification at the northern sampling station, as had previously been inferred by Fish (1957) and Talling (1966; Fig. 11A). Both cross-basin transects May 1995 and April 1996 show warmer waters to the north and cooler waters to the south (Fig. 11). The sampling during May 1995 occurred when winds had intensified with the onset of the southeast monsoon, and the downwelled thermocline intersected the bottom 75 km from Jinja (Figs. 4, 6, 11A). The surfacing of the 6 mg L^{-1} oxygen isopleth by 180 km, the shoaling of the 112 μS cm^{-1} isopleth, and the increased Chl *a* concentrations to the south are consistent with upwelling on the basin scale (Fig. 11A,C,E,G). Elevated specific conductivity and low O_2 were found mid-basin (Fig. 11C,E). These localized changes may be indicative of the effects of other physical processes, such as the gyre observed by Kitaka (1971). The Wedderburn number for the event, $W = g\Delta\rho h^2 \rho^{-1} u_{*w}^{-2} L^{-1}$, computed using average wind speeds, U, of 3.5 m s^{-1} for 7 d at global grid point 1 and Gaussian grid points 1 and 3, one quarter the period of the first internal wave mode of 30 d for Lake Victoria; u_{*w} = 0.001 U; mixed-layer depth (h) = 40 m; length of the lake (L)

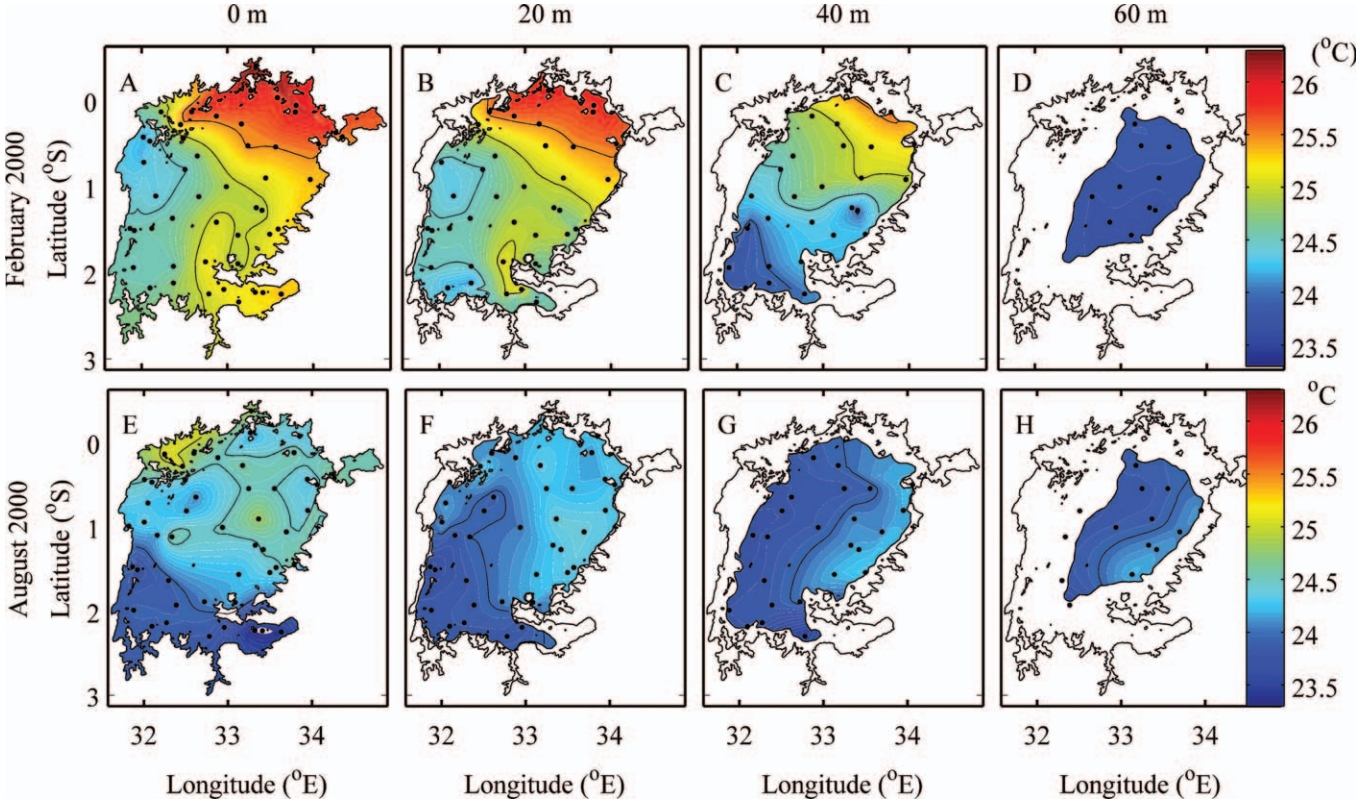

Fig. 12. Temperatures at near-surface, 20 m, 40 m, and 60 m depth in Lake Victoria in February and August 2000. Sampling locations are marked with a black dot. Near-surface temperatures were obtained by averaging from 8–12 m; those at 20, 40, and 60 m are the mean of the data at the depth shown ± 2 m; those for 60 m in August 2000 were obtained by averaging from 52 to 62 m. The near-surface averaging depths were selected to reduce the effects of diel temperature changes and averaging at deeper depths was to obtain data with sufficient spatial resolution for contouring. Contour intervals are 0.05°C; the 24°C, 24.5°C, 25°C, and 25.5°C contours are in black; the coldest temperature illustrated in February 2000 at 60 m was 23.7°C.

= 200 km; and the density difference computed from a temperature difference across the seasonal thermocline of 1.3°C (Figs. 8J, 9), gives a value of 2. This value indicates wind-induced upwelling, and, given the extent of thermocline depression, appears high, with a value slightly less than 1 more likely. Regardless, when the winds relax, it is in the range to induce considerable nonlinearity and mixing (MacIntyre et al. 1999; Boegman et al. 2005; Dorostkar and Boegman 2013). The internal wave-induced mixing, combined with the substantial heat losses (Fig. 6E), likely caused the loss of the seasonal thermocline between the two profiling dates in May 1995 (Fig. 9).

The transect in April 1996 was taken prior to the onset of monsoon conditions and net cooling; to the north and to the south winds were 2–2.5 m s^{-1} (Figs. 4, 6E–H). Stratification across the thermocline was weak, 0.75°C (Fig. 11). The Wedderburn number, computed using the above average wind speeds and temperature difference across the thermocline, mixed-layer depth = 40 m, and length of the lake = 200 km, is in the range 2–4. This result indicates the tilt of the 25°C isotherm results from wind-induced upwelling. Net heat fluxes were similar from north to south and thus, although there is day-to-day variability in the net heat flux, apparently not the cause of the cooler water to the south (Fig. 6E–H; ERA-I, not shown). Secchi depths were shallower and Chl *a* concentrations were higher to the north (Fig. 11). These observations, similar to the values of W, and the near level 2 mg L^{-1} oxygen isopleth at ~ 50 m depth, indicate partial upwelling of the thermocline.

The spatial surveys in February and August 2000 show warmer water to the north, cooler water to the southwest, and overall warmer temperatures in February (Fig. 12). Our sampling in each survey took 2 weeks, with transects beginning to the south and with sampling on some days localized and on others covering ~ 100 km in an east–west direction. With respect to February, the warmer surface temperatures to the northeast result from net heating later in the survey (data not shown) and indicate sampling was not synoptic. Hence, inferences cannot be made regarding movement of gravity currents. The temperature distribution at 60 m is decoupled from the waters above and shows no strong gradients. Hence, water at 60 m may not have warmed much above the previous year's temperature minima.

La Niña conditions prevailed in 2000, and the high winds of the southeast monsoon persisted from May until August at NCEP global grid point 1 and the four Gaussian grid points (Fig. 1A). Surface (net) heat fluxes throughout the monsoon, assuming surface-water temperatures were 25°C, were of order −350 W m^{-2} (−100 W m^{-2}) at all NCEP reanalysis 1 grid points, and, given the uncertainties in surface-water temperature, no south to north gradient in

net heat loss was evident. Monsoon conditions ceased about 10 d earlier mid-lake and farther to the north than to the south. The low surface temperatures to the south result from the net cooling at the start of our sampling (Fig. 12). For the rest of our sampling, there was considerable day-to-day variability with respect to net heat gain or loss but no net heating. Temperatures along the western margin of the basin indicate a progressive increase in the depth of the thermocline separating warm from cool water along an axis from the southwest to the north, with stratification to the north similar to that in July 1995 (Fig. 8D). The earlier cessation of monsoon conditions to the north is the likely cause of the warmer surface temperatures and greater stratification to the north. Because the surface energy budget during the monsoon indicated similar cooling for the lake as a whole, and surface heat fluxes were similar lakewide during our sampling, we infer temperature decreases during the southeast monsoon were larger in the more extensive shallow areas along the western margin of the lake than elsewhere (white areas in Fig. 12F–H). The greater cooling would have induced gravity currents that flowed offshore from multiple locations in shallow areas from the northwest to southwest and caused temperatures to decrease in deeper regions of the lake.

Inshore to offshore transects—Monthly to bimonthly CTD transects from Jinja to the northern offshore station (Fig. 1B) illustrate the changes in stratification over the annual cycle (Fig. 13). Despite sampling beginning earlier in the day at Jinja, inshore water temperatures were 0.2–1.2°C warmer than offshore. Peak seasonal stratification of the upper 10–20 m both inshore and offshore occurred during phase 1 with the 30 August 1995 transect considered in phase 1. Stratification was weaker in the upper water column in phase 2 (January–May) with the seasonal thermocline evident at the offshore stations in January 1995, March 1995, and April 1996. Waters in the first 30 km of the channel were warmer in May 1995 than in March 1995, whereas the 26°C and the 25.6°C isotherms extended farther into Buvuma Channel in May 1995. The warmer inshore waters indicate the cooler waters 20–50 km from Jinja were not necessarily from heat losses at the beginning of the monsoon (Fig. 6). Sustained winds from the southeast began in the week prior to and during our May sampling (Fig. 4D,J). This windstorm, whose magnitude was similar to the one that caused the downwelling illustrated in Fig. 11A, may have advected cooler, offshore water into the embayment. Consistent with this interpretation, the seasonal thermocline was not evident at the northern offshore station. Conditions transitioned to weakly stratified during phase 3 (July 1995), with warmer waters still found inshore and offshore waters 0.5°C cooler.

In all phases, surface overflows toward offshore were possible in the absence of wind due to the warmer surface-water temperatures. As specific conductance is lower in offshore waters, the subsurface decreases in specific conductance in the channel on 07 December 1994, 31 January 1995, 03 March 1995, 30 August 1995, and 21 October 1995 may result from intrusions of offshore water (Fig. 13, lower panels). The lower specific conductance on 20 May 1995 supports our hypothesis that offshore water had been transported into Buvuma Channel. The low specific conductance in much of the water column inshore in phase 3 implies offshore water was advected inshore during windy periods. The temperature and specific conductivity data indicate stratification dynamics were similar inshore and off during all phases of the annual cycle and conditions were favorable for inshore–offshore exchanges.

Thermal stratification of the northwestern archipelago of bays and channels—CTD transects from Napoleon Gulf across Buvuma Channel and through Pilkington Bay (Fig. 1B) from July to November 1994, phase 3 to 1, illustrate the pronounced heating and cooling over diel cycles, the overall cooling from July to August, and the warming and development of seasonal stratification from August to November (Fig. 14). Diurnal heating caused surface-water temperatures to increase by ~ 1°C midday and shallow diurnal thermoclines (23 July, 20 September). Despite the progressive increase in thermal stratification below 12 m from August to November, the warming of the lower water column indicates downward mixing of heat such as could be induced by shear from currents or internal wave instabilities. Horizontal temperature gradients either near the surface or deeper in the water column often formed at the entrance to Pilkington Bay. Spatial variability of wind forcing and surface heating between the bay and the channel along with the morphological constriction between the two water bodies likely contributed to these gradients (Fig. 14). During morning sampling, Buvuma Channel was cooler than the more inshore sites of Pilkington Bay and Napoleon Gulf. The greater cooling in the channel waters was likely caused by higher winds and consequent higher rates of evaporation over open waters combined with somewhat greater diurnal heating in the embayments due to their reduced transparency. Because of the rapid rate of diurnal heating in the Channel, it is not clear whether Pilkington Bay or Napoleon Gulf were persistent sources of heat to Buvuma Channel.

Pilkington Bay temperature, currents, and dissolved oxygen—North–south CTD transects through Pilkington Bay into Buvuma Channel illustrate that diel and seasonal patterns of thermal structure inshore are similar to those in the channel and offshore (Fig. 15). Inshore waters were cooler than mid-bay waters by 0.3–0.5°C in early morning March 1995 (data not shown), May and June 1996 (Fig. 15), and June 1995 (data not shown), but not from July to November 1994 (Fig. 14). The cooler water could flow downslope as a gravity current (e.g., 13:30–14:15 h, 14 May 1996). As stratification built up in the day, currents intensified in the upper water column, with flow predominantly towards Buvuma Channel. The temperatures of inshore waters were not warmer than those offshore in Pilkington Bay; hence, the currents are not indicative of overflows from differential heating within the bay. Flow was from the bay towards the channel throughout most of the day (Fig. 15). The exact flow paths may have been confounded by flows from nearby Hannington Bay, as occurred in April 1996 (MacIntyre et al. 2002). In

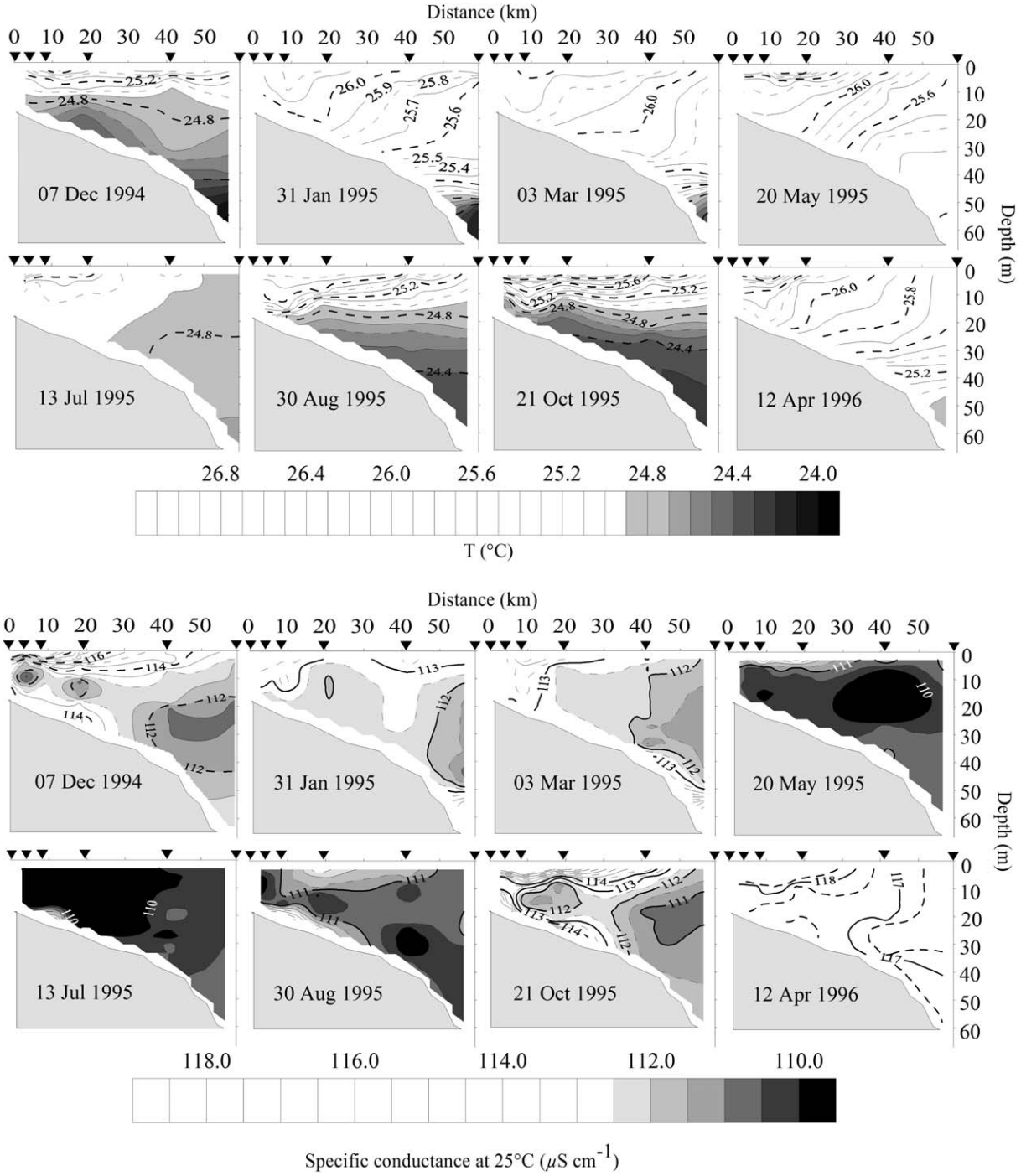

Fig. 13. (Upper panels) Temperature and (lower panels) specific conductance at 25°C on monthly to bimonthly CTD transects at stations 0, 4, 8, 18, 41, and 59 km from Napoleon Gulf to the northern offshore station during 1994–1996. Sampling began offshore of Jinja near 07:00 h, with the typical transit time to the offshore station ~ 2 h. Arrowheads show locations of CTD profiles; temperature contours are 0.1°C; bold dashed reference lines indicate 0.4°C isotherm intervals. Contour intervals for specific conductance are 0.5 μS cm^{-1}.

summary, the diurnal stratification in the inshore bays is conducive to transports into Buvuma Channel. Increased stratification in the day combined with wind intensifies surface currents, and the formation of cool water, as sometimes occurs inshore at night during phases 2 and 3, promotes gravity currents.

Discussion

We have quantified the meteorology and surface energy budget for inshore and offshore waters of Lake Victoria over daily, seasonal, and annual cycles. The associated changes in rates of heating and cooling and wind forcing

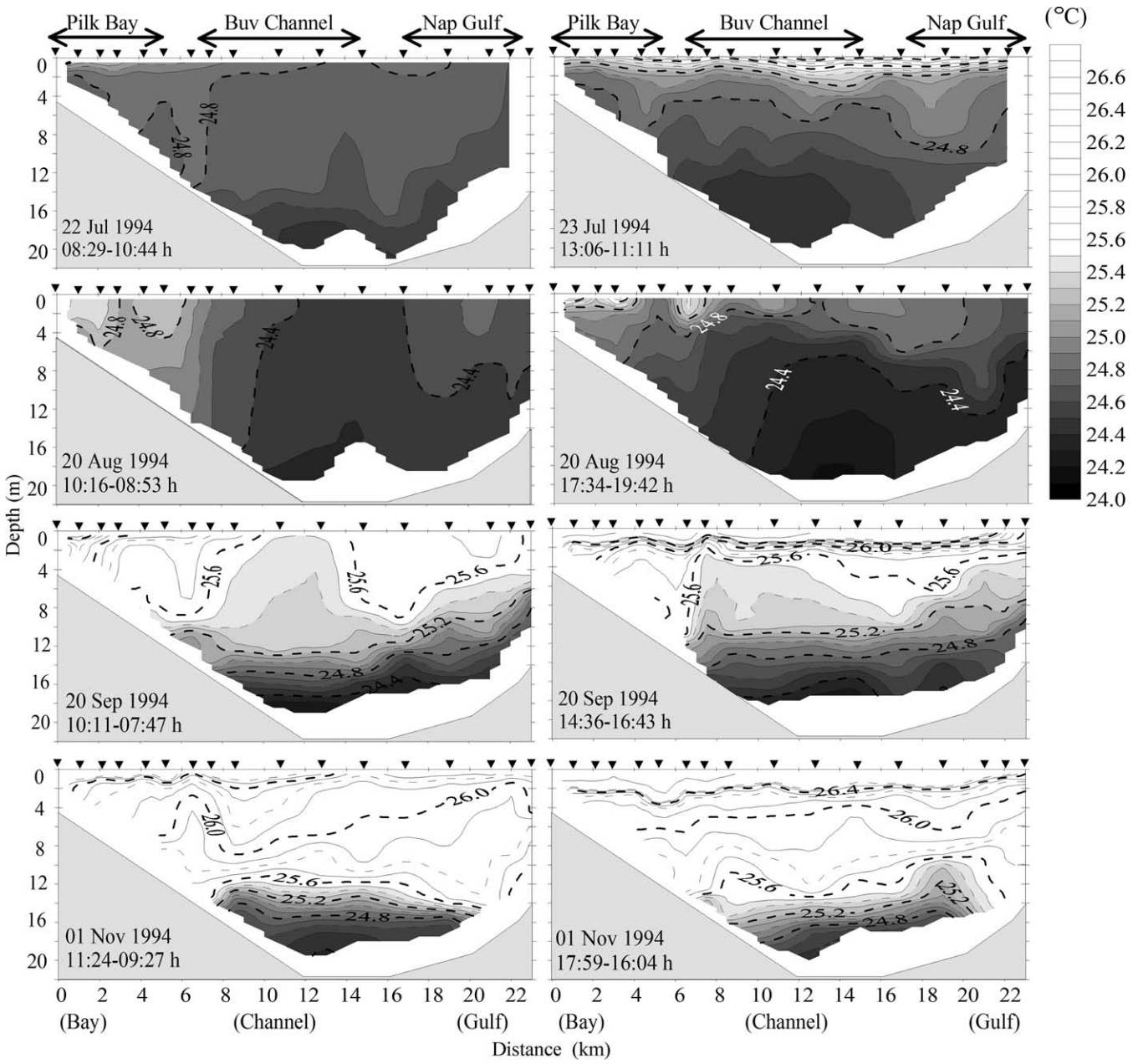

Fig. 14. North–south CTD temperature transects on 22–23 July, 20 August, 20 September, and 01 November 1994 through Pilkington Bay, across Buvuma Channel, and into Napoleon Gulf near the Nile River outflow. The profile time at the northernmost extreme of Pilkington Bay is given first followed by the time of the southernmost profile in Napoleon Gulf.

cause daily and seasonal changes in thermal structure in the northern archipelago and offshore waters and the lakewide differences in thermal structure as illustrated here and in earlier studies (Fish 1957; Newell 1960; Talling 1966). Our cross-basin CTD transects illustrate for the first time that upwelling occurs on the basin scale in response to increased southerly winds over Lake Victoria similar to observations on Lake Malawi and Lake Tanganyika (Spigel and Coulter 1996). The duration and magnitude of winds at the end of the rainy season and during the southeast monsoon are modulated by ENSO cycles. Smaller net heat losses occurred during El Niño years and larger, more sustained ones during La Niña years. In the following, we will examine whether these conditions lead to an underflow of cool water by differential cooling as previously hypothesized (Talling 1966; Cozar et al. 2012). Other basin-scale controls may be operative as well. For instance, the seasonal thermocline forms to the north after the northeast monsoon when winds are southwesterly. Anoxia occurs in Lake Victoria once the lake is thermally stratified (Talling 1966; Hecky et al. 1994), with hypoxic water at the base of the thermocline inshore and offshore. Developing a predictive understanding of controls on the extent of anoxia requires understanding the complex suite of conditions that

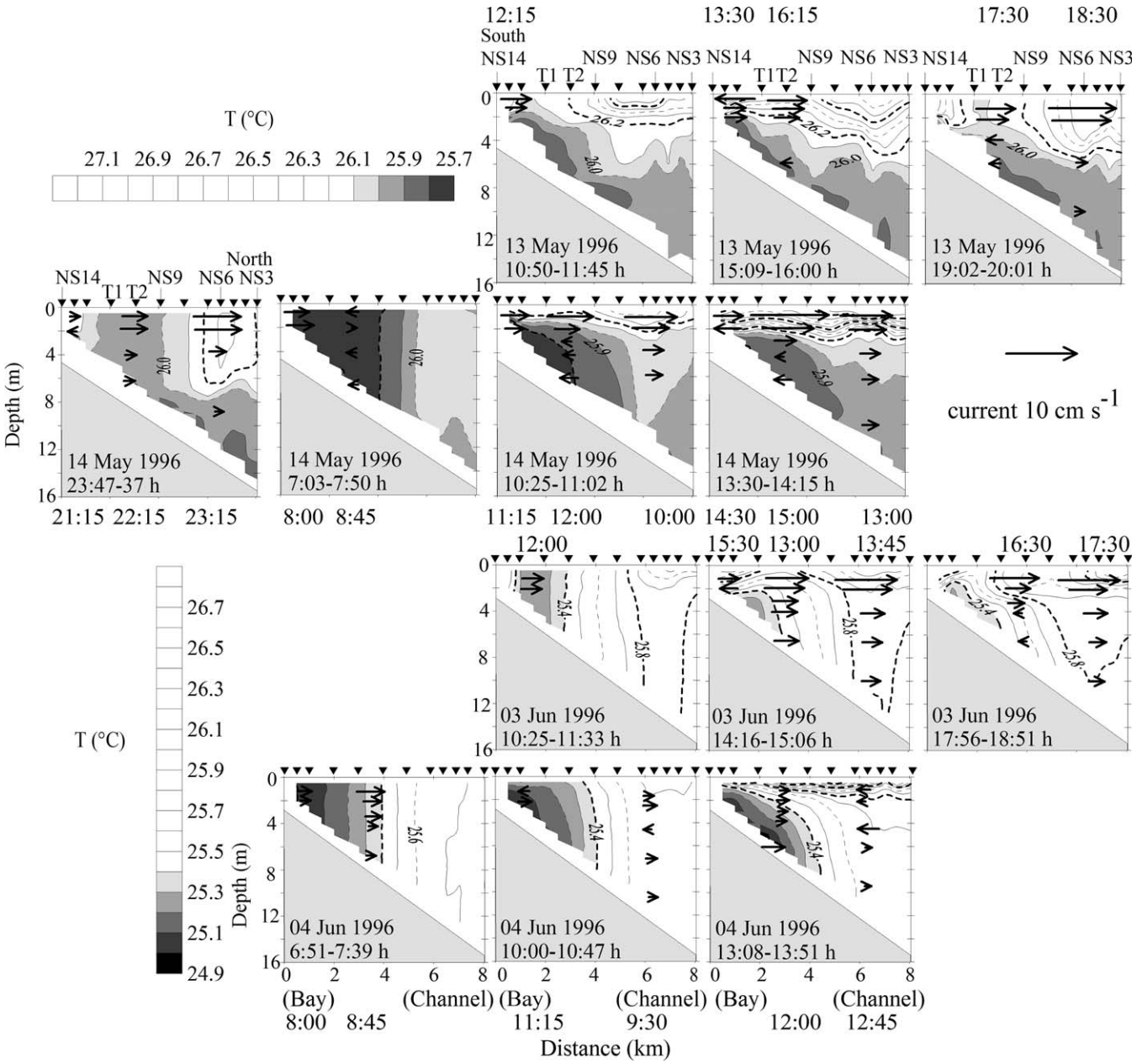

Fig. 15. Temperature contours and velocity vectors from drogue measurements on north–south transects 13–14 May and 03–04 June 1996 through Pilkington Bay into Buvuma Channel. Downward-pointing triangles identify stations whose names increment by one in the southerly direction. T1 and T2 indicate locations of thermistor arrays (data not shown). North–south velocity vectors at Stas. NS14, NS10, and NS6 shown as arrows; direction of arrow indicates current direction along the transect line; times are above the respective vectors and outside the panels. Velocity scale applies to both sampling dates.

moderate the depth and persistence of the seasonal thermocline as well as exchange processes within the lake.

The surface energy budget for Lake Victoria has striking differences relative to those for the Laurentian Great Lakes. Latent heat fluxes are the largest cause of heat loss, with monthly averages up to -300 W m^{-2}, similar to or slightly higher than those in other tropical great lakes (Verburg and Hecky 2003), but with maximal values three times higher than those in the Laurentian Great Lakes when water temperatures are warm (Lofgren and Zhu 2000; Laird and Kristovich 2002). Lakewide and diel variations in latent heat fluxes exceed 100 W m^{-2} in Lake Victoria in contrast to differences of 30 W m^{-2} in the Laurentian Great Lakes. Lakewide temperature differences, however, are $\sim$ 3°C, smaller than the 4–10°C differences across the Laurentian Great Lakes (Goyette et al. 2000). The larger differences in the Laurentian Great Lakes result from the upwelling of cold waters and the large-scale gyres in surface waters (Beletsky and Schwab 2001), which can constrain the extent of horizontal movement and maintain temperature differences. The large latent heat fluxes and diel variability contribute to deeper nocturnal and seasonal

mixed layers in Lake Victoria and the other African Great Lakes relative to the Laurentian Great Lakes, and the spatial variability in latent heat fluxes creates conditions conducive for horizontal convective circulation (Talling 1963; Verburg et al. 2011; Cozar et al. 2012). Gyre structures are also present in Lake Victoria, and three-dimensional hydrodynamical modeling indicates these features will contribute to, rather than constrain, horizontal exchanges (Song et al. 2004).

Our combined heat budget and temperature data support the hypothesis that horizontal convective exchanges occur over large and small scales in Lake Victoria. However, the pronounced diel variability in heating and cooling, the diel changes in wind direction and magnitude, and increased winds during phases 2 and 3 could disrupt or overwhelm lateral convection. To develop generalities regarding horizontal exchanges in tropical lakes, we evaluate processes that contribute to inshore and offshore exchanges in Lake Victoria, address how exchanges would vary seasonally, and further evaluate whether large-scale gravity currents, similar to those in Lake Albert (Talling 1963) and Lake Tanganyika (Verburg et al. 2011), contribute to the stratification dynamics of Lake Victoria.

Processes and exchanges in nearshore embayments—Greater nocturnal cooling inshore may lead to formation of gravity currents, which then flow into Buvuma Channel (Fig. 15). The apparent slumping of these cool waters, however, could also be explained by the rapid warming that occurs in Pilkington Bay. Only on early afternoon 14 May 1996 do we see the cool water from Pilkington Bay extend into the channel connecting this embayment with Buvuma Channel. Without sustained time-series measurements, the importance of gravity currents remains equivocal. In the upper water column, greater heating does not occur inshore, but instead warmer waters are more consistently found in the connecting channel. Thus, the outgoing water masses in the channel do not occur because of buoyant overflows from differential heating within Pilkington Bay. Surface currents are intensified by heating, as observed by Ochumba (1996). The surface flows are predominantly northward, suggesting the lake breeze contributes to their setup and persistence, similar to observations in Evans (1961). Flows are generally out of the connecting channel and into Buvuma Channel regardless of time of day, suggesting, as in MacIntyre et al. (2002), that flows from Hannington Bay also contribute to exchange. The horizontal temperature gradients are at most a few tenths of a degree, indicating the export of heat will be minimal. Assuming the outflows occur over half a day, the net discharge though the connecting channel to Buvuma Channel from the upper 2 m alone is 120 $m^3\ s^{-1}$. This value is consistent with the computed net annual discharge from Winam Gulf of 35 $m^3\ s^{-1}$ (Njuru 2008). Gikumu-Njuru et al. (2013) find nutrients are retained in Winam Gulf and the main basin is a source of phosphorus for the gulf. Concentrations of chlorophyll and of particulate nitrogen and carbon in embayments such as Pilkington Bay are higher than in offshore waters (Ramlal et al. 2001; Hecky et al. 2010). With the higher exchange from Pilkington Bay, and the exchanges from Buvuma Channel to be discussed in the following, our results are in contrast to those in Gikumu-Njuru et al. (2013) and indicate a net efflux from the northern archipelago will contribute to eutrophication farther offshore.

Exchanges between larger channels and the main lake—With greater heating inshore (Fig. 5) and generally similar rates of cooling at night, $-100\ W\ m^{-2}$, both inshore and offshore (Fig. 3), lateral convection is expected to induce exchange via buoyant overflows offshore. The transects along Buvuma Channel support this inference, as they indicate warmer water is inshore, despite the earlier start of sampling inshore than offshore (Fig. 13). The changes in conductance with depth are small and near the resolution of the CTD, but persistently indicate mid-water intrusions of lower-conductivity water, as found offshore, during phase 1 and below 10 m during phase 2. These patterns provide support for inshore–offshore exchange. At steady state and neglecting vertical mixing, current speeds induced by horizontal temperature differences can be estimated as $u \sim (g\alpha\Delta Th)^{1/2}$ where g is gravity, α is the coefficient of thermal expansion, ΔT is the horizontal temperature difference (°C), and h is the intrusion thickness (Monismith et al. 1990; Nepf and Oldham 1997). Assuming the depth of the diurnal thermocline was ca. 5 m and horizontal temperature differences were ca. 0.4°C yields a current velocity estimate of ca. 0.07 $m\ s^{-1}$. Assuming surface drift velocities are approximately 3% of the wind speed, such currents would be induced by winds of 2.6 $m\ s^{-1}$. Thus, wind will augment exchange of warmer surface waters offshore during land breeze conditions, but would overwhelm such circulations during lake breeze conditions.

For persistent horizontal temperature differences, the decrease in mass flux as vertical mixing increases can be determined from the dimensionless parameter GrA^2, where Gr is the Grashof number and A is aspect ratio H : L where H is depth and L is length (Ivey 2004). $Gr = g'H^3\ K_z^{-2}$ where g' is $g\ \Delta\rho\ \rho^{-1}$ where g is gravity; ρ is density; $\Delta\rho$ is the horizontal density difference, which in freshwater systems such as Lake Victoria is due to temperature; and K_z is the coefficient of eddy diffusivity, which characterizes the potential for vertical mixing. For $GrA^2 = 1000$, the flux would be 60% of that with no mixing, and for $GrA^2 = 1$, the fraction would be less than 5% (Ivey 2004). Temperature gradients are least across the channel during phases 1 and 3, ~ 0.5°C. They increase during phase 2 from initial values of 0.7°C to maximal values of 1.6°C. Assuming $\varepsilon = 10^{-7}\ m^2\ s^{-3}$, as typically occurs in stratified flows with some internal wave activity (MacIntyre et al. 2009), and calculating K_z as $\Gamma\ \varepsilon\ N^{-2}$ (*see* Methods), K_z for the stronger vertical stratification in phase 1 equals $1.5 \times 10^{-4}\ m^2\ s^{-1}$ and for the weaker vertical stratification in phase 2 equals $4 \times 10^{-4}\ m^2\ s^{-1}$. These are relatively high values of K_z and result from the overall weak channel stratification and assumption of moderate turbulence. Assuming cross-basin temperature differences of 0.6°C and 1.6°C, mean channel depth H of 30 m, and channel length L of 50 km, values of GrA^2 during phase 1 would be of order 700 and during phase 2 would be 300. Hence,

overflows of warmer water to offshore locations could occur but the mass flux would be 40–50% of that in the absence of vertical mixing (Ivey 2004). During periods with low winds and less vertical mixing, the fraction exchanged would be higher. As discussed above, flows from the northern offshore waters will be augmented during land breeze conditions but blocked when winds come from the south with velocities exceeding ~ 3 m s^{-1}. Despite these caveats, net transport of heat from inshore waters is expected.

Internal wave motions can also induce exchange. Fish (1957) computed a 30 d seiche period in Lake Victoria, and Song (2000) computed a 30 d period and observed rotation in the internal wave field. Fish (1957) observed synchrony of isotherm displacements between inshore and offshore sites and inferred that long waves propagated inshore in the lower water column. The mid-water intrusions of low conductance water in December 1994, August 1995, and October 1995 may be the signature of internal wave-induced exchange with offshore flow in the upper and lower water column. Late in phase 1, water in the lower water column of the channel is hypoxic (data not shown), and offshore flows would export regenerated nutrients and dissolved gases. Because of the lake–land breeze and sometimes westerly flows, wave periods may be shorter and exchanges more frequent by this mechanism than Fish predicted (Newell 1960). During phase 2, when the seasonal thermocline is present, relaxation of a downwelled thermocline (Fig. 11A) may induce upslope flow (Venayagamoorthy and Fringer 2007). Our data set is too intermittent to show the oscillatory flows that would provide support for internal wave driven flows in the channel, but internal waves will be generated on relaxation of the downwelled thermocline in the main basin during phase 2 (Fig. 11). The changes in wind velocity in the reanalysis data indicate downwelling followed by upwelling would occur one to several times during phase 2 (Fig. 4). Internal wave-induced exchanges can be considerable; 40% of the hypolimnetic waters in the southwestern embayment of Lake Geneva can be exchanged during incursion of basin-scale waves (Umlauf and Lemmin 2005).

Inshore–offshore exchange may be mediated when winds are sustained for several days and induce flushing. During high winds, a large volume of surface water may be pushed inshore, where it mixes with channel waters with offshore flow on relaxation of the wind. The northward movements of the 26°C and 25.6°C isotherms in response to the sustained winds in May 1995 (Fig. 4D,J) are indicative of the onset of flushing (Fig. 13). Similarly, the low conductance water found inshore in July 1995 (Fig. 13) in phase 3 and Fish's (1957) phytoplankton counts at inshore and offshore stations provide evidence for flushing. Fish (1957) observed that the abundance of *Nitzschia* tended to be less than 200 cells cm^{-3} offshore but increased to 800 cells cm^{-3} when offshore waters became isothermal in January 1953. As isothermy in northern offshore waters results from downwelling of the seasonal thermocline offshore due to high winds, the wind-induced flushing of the inshore embayments likely transported *Nitzschia* from inshore where abundances exceeded 1700 cells cm^{-3}. The largest, most rapid exchanges between the channel and offshore waters would occur during flushing events.

The processes dominating inshore–offshore exchange will vary seasonally. The inshore–offshore temperature differences indicate lateral convection could occur year round. To the north, these will be supported by the land breeze from June until November (Fig. 1A). Internal wave-mediated exchanges can occur whenever the water column is stratified. These flows are oscillatory and would not induce net transport unless nonlinear (Maderich et al. 2001); however, they would cause shear, which contributes to vertical mixing. Assuming an inflow of water from offshore, the mixing may help delay the development of anoxia in the lower water column inshore. Once the stronger southerly winds commence in April or May, flushing or internal wave motions would cause greater exchanges to the north, with convective flows resuming when wind directions shift.

Spatial–temporal variations in surface energy budgets, cross-basin exchanges, and extent and persistence of hypoxia—A long-standing question has been when and how two-dimensional processes cause changes in mixed-layer depth and stratification at the northern offshore station of Lake Victoria (Fish 1957; Talling 1966; Coulter and Spigel 1991). Of related importance are controls on the extent of hypoxia, with both one- and two-dimensional processes of importance. In the following, we focus on three important hydrodynamic processes and discuss implications for extent and persistence of hypoxia. The first is nocturnal mixing at the northern offshore station due to moderate winds at night at the onset of phase 1. The second is the formation of the seasonal thermocline at the onset of phase 2. The third is differential cooling during phase 3.

Wind-induced mixing at night: Consequences for hypoxia—Increased nocturnal winds and associated increased latent heat fluxes will mix heat downwards and contribute to ventilating the lower water column. The deepening of the 25°C isotherm and the warming of the water below are indicative of mixing at the onset of phase 1 in 1994 (Fig. 9). Heat was similarly mixed downwards in Buvuma Channel (Fig. 14). The time-series wind data imply the mixing was induced by moderate winds and increased latent heat fluxes at night at the onset of phase 1 in 1994 (Figs. 4E,F, 6A; ERA-I data, not shown). When winds are lower, evaporation rates are less and heat will accumulate in the upper layers. Unfortunately, our temperature profiling was insufficient to detect this consequence in 1995, but it is evident in data from 1991 (R. Hecky, pers. comm.). When the lower water column is isolated, oxygen concentrations will decrease more rapidly for the same respiration rates. In support of this hypothesis, the 3 mg L^{-1} isopleth was 15 m deeper in the October sampling of 1994 than in 1991 and 1995 (data not shown). Thus, we infer that when winds are lower at the end of the southeast monsoon through the onset of the rainy season, latent heat fluxes and vertical mixing are reduced and oxygen concentrations will decrease over a larger volume of the lake.

Formation of the seasonal thermocline—The seasonal thermocline forms in phase 2 (Fig. 9). Because of discrepancies between the NCEP and ERA-I heat budgets, it is unclear whether the deepening is in part driven by heat loss (Fig. 6E). However, we contend that the seasonal thermocline that forms and persists to the north results from downwelling induced by sustained southwesterly and later southeasterly winds (Fig. 4). As described previously, the light southerly winds in April 1996 induced downwelling to the north, as did the stronger winds in May 1995 (Fig. 11). Wedderburn numbers were of order 2 or less. Winds were of similar or higher magnitude than those in April in January 1995 and 1996 (Fig. 4). With similar stratification, Wedderburn numbers were in the range indicating these winds would cause downwelling and thus induce the seasonal thermocline to the north. Prior to the high winds in May, winds either intensify or reverse direction on monthly time scales or less thus moderating thermocline depth (NCEP and ERA-I data). These observations support Fish's (1957) and Talling's (1966) contentions that isothermy in January 1953 and 1961 was due to thermocline tilting and similarly may explain the isothermy found by Fish later in phase 2 in 1953. Wind speeds increased more rapidly in 1995 than in 1996, and the seasonal thermocline was deeper in early 1995 (Fig. 9). Concentrations of oxygen were less than 2 mg L^{-1} below 50 m in early February 1995 and 40 m in February 1996. Consequently, the changes in the surface energy budget and wind during phase 2 moderate the depth of the seasonal thermocline and depth of hypoxia.

Cross-basin transports and vertical mixing after the seasonal thermocline forms would result from shifts in wind direction. Southerly flow in the upper water column would occur on relaxation of the winds. For sufficiently low Wedderburn numbers, mixing would occur within the thermocline as a result of shear from nonlinear internal waves (Boegman et al. 2005). In addition, progressive nonlinear waves would form, and, depending on the spatial extent of the thermocline (Figs. 10F, 11), traverse the full or part of the basin, and transport solutes, gases, and particles southward within the thermocline (Mortimer and Horn 1982; Maderich et al. 2001). As evidence for the mixing, stratification to the north in May 1995 was considerably weakened after the wind event (Figs. 9, 11A) and hypoxia relieved (data not shown). Internal wave-induced mixing when wind speeds typically rise (Fig. 4) may be another mechanism besides cooling (Fig. 8A–C) that leads to the breakdown of stratification to the north (Fig. 9). It is unclear how long the seasonal thermocline would persist. Surprisingly, a north to south thermocline tilt was present in June 1957 (Fig. 10B) despite high winds at the end of the rainy season in that year (NCEP reanalysis 1 data, not shown). Underflows associated with the greater cooling to the south during the southeast monsoon (Figs. 5, 6) could maintain stratification and enable exchanges via internal wave activity.

Cross-basin exchanges: Underflows—Temperature decreases by up to 0.4°C at depths below 30 m have been observed to the north in our study and earlier ones towards the end of the southeast monsoon (Fig. 9; Fish 1957; Talling 1966). In the following, we assess whether localized net heat losses or heat losses followed by gravity current formation at the regional or basin scale caused deep-water cooling. Alternatively, relaxation of cross-basin isotherm tilting may have caused the presumed underflows. Mean lake temperatures decreased by 0.4°C from late July to late August 1994 and 0.1°C from mid-July to late August 1995. In 1994, net heat fluxes were near zero from July to August when the cooling occurred (Fig. 6E; and *see* Stratification of northern offshore waters); hence, advective flows of cool water are required to explain the temperature decrease. The calculations in Table 2 support this inference, as do the net heat fluxes at grid point 1 computed from the ERA-I data (not shown). Although the north to south differences in net heating could support differential cooling on the basin scale (Fig. 6 and ERA-I heat budget), cooling in shallow regions to the northwest could also contribute to underflows. For example, using the one-dimensional equation for temperature change, $dT/dt = -H/(c_p \rho D)$, where T is temperature, t is time, H is net heat flux, c_p is specific heat capacity, ρ is density, and D is depth, and assuming full water column mixing inshore to 20 and 40 m and offshore to 65 m, temperatures would decrease by 1.5°C, 0.8°C, and 0.5°C for net cooling of -50 W m^{-2}, as occurred several times in 4 d average ERA-I results for July and August 1994. The greater cooling in shallow regions could induce gravity currents that flow offshore. The tilted isotherms from Sta. M to N in August 1957, although possibly confounded by inflows from the Kagera River, provide an example of cooler nearshore waters (Figs. 1, 10). In contrast, in 1995, net cooling was ~ -25 W m^{-2} from July to August. During July 1995, the net heat losses computed locally would cause temperatures to decline 0.2°C, more than the measured change. The cooling in the lower water column from July to August 1995 can be explained by local processes. Thus, in some years localized cooling can explain the temperature decreases and in other years regional cooling and the resulting cool-water gravity currents.

Lake Victoria's bathymetry is more likely to induce cooling to the west for the same net heat losses across the lake. The western side has extensive regions with depths shallower than 20 m, and the 60 m contour is 90 km offshore. In contrast, it is 25 km offshore to the east and 60 km offshore to the south. Hence, cold water formation will be greater to the west, as illustrated in Fig. 12. Gravity currents are expected from the west and northwest because of the more extensive shallow regions there and from the south because of the shallower bathymetry and greater net heat losses. Cool waters could also originate inshore. Nocturnal mixing in August 1994 caused the temperatures in Buvuma Channel to be near uniform at 24.5°C (Fig. 14), slightly warmer than the temperature at 60 m at the northern offshore site when the lake restratified (Fig. 9). Temperatures in 30 m deep Roseberry Channel, the southwestern extension of Buvuma Channel, were 23.6°C below 22 m in August 1953, cooler than those found offshore at depth. Interestingly, abundance of *Melosira*, now *Aulacoseira nyassensis* var. *victoriae* (J. F. Talling pers. comm.), prevalent in near-bottom waters of Buvuma Channel, increased to $\sim$ 1500 cells mL^{-1} at 60 m but not in the overlying water when the near-bottom waters cooled

offshore in August 1952 and 1953 (Fish 1957). Irradiance at 60 m would be insufficient for growth. Increased abundance of this diatom offshore supports our contention that flows of cool water from shallower locations to the northwest can contribute to the stratification dynamics of Lake Victoria.

Horizontal convective circulation on the basin scale, as in Verburg et al. (2011), has been hypothesized to contribute to the cooling that occurs below 30 m late in the monsoon in northern waters. This mechanism requires, as in Verburg et al. (2011), greater heating at one end of a lake than at the other. Cozar et al. (2012) computed that the temperature differences from north to south across Lake Victoria are sufficient to sustain a horizontal convective circulation in months, such as August to November, with low average wind speeds, and water warmer to the north by 0.5°C. Assessment depends on the value of the dimensionless parameter (B), which is a ratio of wind-induced to buoyancy-induced flows. $B = abs(u_*L/\alpha\Delta T g h^2)$ where u_*, the water friction velocity, α, and g were defined earlier, L is length of the lake, ΔT is temperature difference across the lake, and h is the vertical dimension of the horizontal convective cell. For L = 200 km, h = 60 m to allow for the observed intrusions of cool water, ΔT = 0.2°C and 0.5°C, as Cozar et al. (2012) obtained as monthly average of day and night remotely sensed data, and mean winds of 2 m s^{-1}, similar to what Cozar et al. (2012) used as monthly averages, B = 0.4 and 0.2. For winds of 0.5 m s^{-1}, as occurred at night to the north in August to November 1994, B = 3 and 1. Values of $B \ll 1$ imply horizontal convective circulation dominates. The values of B computed here are of order 1 and 0.1 and imply both wind and horizontal convection contribute to the flow. Vertical mixing early in the monsoon would preclude development of gravity currents. At that time, Kz $\sim$ = 0.7 m^2 s^{-1} (*see* Diurnal and seasonal stratification), and, following Ivey (2004), for a horizontal temperature difference of 0.5°C, $GrA^2 \ll 1$. Vertical mixing would disrupt the convective flows and mass transfer would be minimal. For the increased stratification later in the southeast monsoon (Figs. 8D, 9), K_z is of order 1×10^{-4} m^2 s^{-1}, GrA^2 is $\sim$ 2000, and mixing would not disrupt the hypothesized horizontal convection. Despite such flows being possible, the asymmetry in basin shape that induces gyres in the northern and southern halves of the lake (Song 2000) may confound the requisite surficial southerly flow needed to complete the circulation.

Whether horizontal convective circulation occurs on the basin scale after the southeast monsoon remains equivocal for other reasons. Net heating to the north and net cooling to the south is an expected component of horizontal convective circulation. The heat budget derived from the NCEP reanalysis 1 data shifts immediately after the monsoon to conditions of net heat fluxes being either negative or zero to the north and net heat gain to the south and east (Fig. 6). The heat budget from ERA-I indicates a more rapid onset of heating to the north in some years but not others and that the duration of cooling to the south relative to the north is highly dependent upon assumed temperatures. The monthly data also show increased net heat fluxes in September and more positive net heating in the day to the south than the north, and suggest warmer water would form to the south (Fig. 5). The water surface temperatures from ERA-I heat more rapidly at southern as opposed to more northerly grid points in September (data not shown). These conditions would lead to advection of heat to the northern waters of the lake, as opposed to the southerly flow proposed in Cozar et al. (2012). Thus, the evidence is equivocal for horizontal convective circulation on the basin scale at the end of the southeast monsoon. The surface energy budgets do indicate greater cooling to the south, which could support differential cooling on the basin scale.

For transports over large spatial scales by deep-water gravity currents induced by differential cooling, advective time scales must be shorter than time scales of mixing and time scales of entrainment. Comparison of advective and mixing time scales, $\tau_{adv} = L/u$ and $\tau_{mix} = l^2/K_z$, respectively, where u is velocity, L is the distance traversed by the gravity current, and l is the size of turbulent eddies or overturns, allow assessment as to whether an intrusion would be mixed into the overlying water as opposed to moving laterally a defined distance. For ΔT = 0.25°C, as observed between inshore and offshore waters near Bukoba (Fig. 10C), letting h be 15 m, the vertical extent of the intrusion, and using the equation $u \sim (g\alpha\Delta Th)^{1/2}$ discussed above, the velocity of gravity currents is of order 0.1 m s^{-1}. The advective time scale, τ_{adv}, for an intrusion to flow 50–100 km is 6–12 d. Assuming a larger ΔT = 0.5°C as in Cozar et al. (2012) and a deeper layer of cool water, h = 35 m, velocity is of order 0.2 m s^{-1}. For deep-water gravity currents traversing L = 200 km, τ_{adv} is 12 d.

Using our observations that full overturn does occur at the northern station and l is 60 m (Fig. 8C), K_z = $\sim$ 0.7 m^2 s^{-1} (*see* Diurnal and seasonal stratification) and τ_{mix} = 1 h, $\tau_{mix} \ll \tau_{adv}$. Thus, when winds intensify at the end of the rainy season and during the southeast monsoon when heat loss is considerable, gravity currents would be disrupted by mixing. N $\sim$ = 3 cph between 20 m and 40 m during July 1995 (Fig. 8E). Assuming ε of 1×10^{-7} m^2 s^{-3}, a high value for a location deep in the water column, gives $K_z = 7 \times 10^{-4}$ m^2 s^{-1} (*see* Diurnal and seasonal stratification). Using l = 10–20 m (Fig. 8F), τ_{mix} is 2–7 d, an order of magnitude longer if ε were 10 times less. τ_{mix} and τ_{adv} are of similar magnitude in the latter half of the southeast monsoon, which implies that the gravity currents would be mixed into ambient water unless K_z is lower than in our estimate. An alternate approach is to determine the time scale for entrainment, τ_{ent}, which also applies once the water column has stratified. $\tau_{ent} = h^2N^2/\beta$ (Turner 1973). For h = 50 m, N = 3 cph, and a maximum net heat flux observed to the north, -100 W m^{-2} (Fig. 6E; 1996), $\beta = 6.6 \times 10^{-8}$ m^2 s^{-3}, and τ_{ent} is 12 d. Again, during the highest winds when such large heat fluxes are observed, τ_{adv} is similar to τ_{ent} and gravity currents would be mixed into the overlying water. When wind speeds drop and 10 d average net heat fluxes decrease to less than -50 W m^{-2} (Fig. 6), τ_{ent} doubles. Under those average conditions, gravity currents would not be entrained by thermals induced by cooling. However, if intermittent winds cause near-bottom intensification of shear and mixing as implied in Fig. 8F, gravity currents could be dispersed.

Isothermy has been observed in temperature profiles only in late June and early July during the southeast monsoon (Fish 1957; Talling 1966; this study), and nutrient profiles taken from the north after early July show near-bottom stratification during the southeast monsoon (Talling 1966). From these observations and from the surface energy budget in Fig. 6, we infer that isothermy in northern waters tends to occur early in the southeast monsoon but not later in the monsoon. Hence, this analysis combined with observations implies that gravity currents can persist and cause the observed cooling deeper in the water column. Based on the complexity of Lake Victoria's shoreline and the asymmetry in basin morphometry, we argue that a defined horizontal convective cell is unlikely to be generated as in Lake Tanganyika (Verburg et al. 2011). Instead, we argue that gravity currents that transport cool water offshore form in multiple locations. Differential cooling causes gravity currents that flow at depth, but wind-driven circulation contributes to redistributing heat in surficial waters.

Interannual variability in gravity current formation is likely linked to ENSO cycles as they influence the duration of high winds over the basin and the magnitude of heat fluxes. In 1995, an El Niño year, the temperature decrease in the lower water column was similar to that expected from the local, net heat losses whereas in 1994, a normal year, advection was required to balance the heat budget. Net heat losses were larger and more persistent to the south during 1996, a La Niña year, and even greater in 2000 (data not shown), a strong La Niña year. These differences will influence the extent to which the lake cools and the tendency for advective flows from differential cooling. How the differences will influence oxygen concentrations in near-bottom waters requires investigation. For instance, oxygen concentrations remained above 4 mg L^{-1} (data not shown) at the depths where the lower water column cooled in August 1994 and 1995, suggesting a short residence time for the near-bottom waters and supporting our inference of relatively high K_z. In contrast, oxygen concentrations decreased to values less than 3 mg L^{-1} below 55 m, where water temperatures decreased in August 1952 and August 1953 (Talling 1966). Winds during the southeast monsoon were higher in those years (Meteorological Department of the East African High Commission; NCEP reanalysis I data). If the gravity currents were cooler and resulting temperature gradients larger, near-bottom mixing may have been less. Assuming oxygen consumption is rapid, deoxygenation would persist.

Alternatively, restratification towards the end of the southeast monsoon results from relaxation of a downwelled thermocline. Thermocline tilting would be sustained for the duration of the sustained southerly winds, as in Figs. 10C northerly leg, 11A, with warmer isothermal water to the north and cooler, weakly stratified water to the south. The restratification typically observed in either July or August would then result from the thermocline moving northwards on relaxation of the southerly winds. The oxygen data from Fish's (1957) and Talling's (1966) surveys support this inference, as the low oxygen concentrations were observed shortly after periods of isothermy and, in 1953, with a 1 month periodicity. The stability of stratification and oxygen concentrations would then depend on not only mixing due to heat loss at the surface but mixing in the lower water column associated with the internal wave motions. The timing of the apparent restratification to the north would depend on ENSO cycles, as they moderate the duration of the sustained southeasterly winds.

In summary, rates of heating and cooling and wind forcing vary spatially and temporally over Lake Victoria. On the scale of kilometers, that is, for the inshore embayments, nocturnal cooling causes cooler waters inshore that may flow offshore as gravity currents during phases 2 and 3. Daytime heating stratifies the upper water column and intensified wind-induced currents transport substantial quantities of water out of the embayments. On the scale of tens of kilometers, that is, the size of channels connecting inshore and offshore waters, temperatures are warmer inshore than offshore. The temperature differences are large enough to induce flow. Despite vertical mixing, net persistence of the offshore flow of heat in buoyant overflows is expected except when winds are sustained from the south. Flushing of inshore embayments will be most extensive on relaxation of sustained southerly winds at the onset of and during the southeast monsoon. On the basin scale, stratification is induced when advective flows are generated by spatial differences in heating and cooling and can be intensified or reduced to the north when sustained southerly winds cause downwelling. If gravity currents form at multiple locations along the margins of Lake Victoria, the onset of stratification at the end of the southeast monsoon would be similar to that described by Wells and Sherman (2001) for smaller water bodies during winter conditions. Uncertainty remains as to the cause of the apparent cool water underflows. If the full water column does not mix during the southeast monsoon and stratification is due to relaxation of cross-basin upwelling, between-year variability in stratification and oxygen dynamics will not only depend on wind and cooling but will also depend on lake depth as it varies with rainfall (Birkett et al. 1999). In contrast to temperate lakes where the seasonal cycle of stratification is driven by processes that are largely one-dimensional (Yeates and Imberger 1994), advection contributes in Lake Victoria with wind-induced thermocline tilting and associated mixing a further control.

This mechanistic understanding of the physical limnology of Lake Victoria provides a basis for predicting inshore–offshore and basin-scale exchanges. The 2 years of time-series temperature and meteorological data that are the primary focus of this study begin to illustrate between-year variability related to atmospheric cycles such as ENSO, which warrants further exploration. For example, the extent to which nocturnal winds to the north at the end of the southeast monsoon are enhanced moderates heat loss. These winds appear to depend on ENSO cycles. The extent of the cooling moderates the downward mixing of heat and oxygen into the lower water column and, through controls on mixed-layer depth, will moderate the depth of anoxia. Measurements of oxygen

concentrations have largely been made at the northern offshore stations. As downwelling of the thermocline to the north varies with the intensity of sustained southerly winds, prior inferences as to the volume of anoxic water within the lake need to be interpreted in the context of internal wave dynamics. Coupled regional climate models with three-dimensional hydrodynamic models using simplified basin geometry (Song et al. 2002, 2004; Anyah et al. 2005) have quantified flows during the short rains. This study points to the importance of including nearshore regions in modeling, for modeling during other seasons, and for assessing how the variability due to ENSO cycles modifies the extent of vertical mixing and horizontal exchanges with consequences for nutrient fluxes, the volume of anoxic waters, and productivity of the plankton and fisheries.

Acknowledgments

We give special thanks to Patricia Ramlal, who coordinated and conducted field work from 1994 to 1996. We thank Fred Bugenyi, Rose Mugidde, Moses Magumba, Richard Ogutu, and the captain and crew of the R/V *Ibis* for their support in the field and in the laboratory, G. W. Kling for encouragement and support, and J. F. Talling, J. M. Melack, G. W. Kling, P. Verburg, and one anonymous reviewer for providing critical comments on various drafts of the manuscript. Peter Njuru provided morphometric data for the northern inshore waters. The Fisheries Research Institute in Uganda provided permission, financial support, and help in multiple ways. We thank J. F. Talling for providing the 1957–1958 lakewide data. John Lenters and Evren Soylu provided the ECMWF ERA-I data. The Ugandan Water Development agency provided the 1994–1996 Entebbe meteorology, lake level, and Nile outflow discharge data. Financial support was provided by National Science Foundation (NSF) grants Division of Environmental Biology (DEB) 95-53064, 93-18085, 93-17986, 97-26932, 01-08572, 06-40953, Ocean Sciences (OCE) 99-06924, by an NSF DEB grant to J. T. Lehman, by the Centre for Water Research, University of Western Australia for J. Romero, by an internship to G. Silsbe from the Canadian International Development Agency with logistic support provided by the European Union Lake Victoria Fisheries Project, and by a Blaustein Visiting Professorship from the Department of Environmental Earth System Science, Stanford University, to S. MacIntyre.

References

Anyah, R. O., F. H. M. Semazzi, and L. Xie. 2006. Simulated physical mechanisms associated with climate variability over Lake Victoria Basin in East Africa. Mon. Weather Rev. **134:** 3588–3609, doi:10.1175/MWR3266.1

Beadle, L. C. 1981. Inland waters of tropical Africa. Longman.

Bednarz, T. P., C. Lei, and J. C. Patterson. 2009. Unsteady natural convection induced by diurnal temperature changes in a reservoir with slowly varying bottom topography. Int. J. Therm. Sci. **48:** 1932–1942, doi:10.1016/j.ijthermalsci.2009.02.011

Beletsky, D., and D. J. Schwab. 2001. Modeling circulation and thermal structure in Lake Michigan: Annual cycle and interannual variability. J. Geophys. Res. **106:** 19745–19771, doi:10.1029/2000JC000691

Birkett, C., R. Murtugudde, and T. Allen. 1999. Indian Ocean climate event brings floods to East Africa's lakes and the Sudd Marsh. Geophys. Res. Lett. **26:** 1031–1034, doi:10.1029/1999GL900165

Boegman, L., G. N. Ivey, and J. Imberger. 2005. The degeneration of internal waves in lakes with sloping topography. Limnol. Oceanogr. **50:** 1620–1637, doi:10.4319/lo.2005.50.5.1620

Brainerd, K. E., and M. C. Gregg. 1993. Diurnal restratification and turbulence in the oceanic surface mixed layer. 1. Observations. J. Geophys Res. **98:** 22645–22656, doi:10.1029/93JC02297

Brock, T. D. 1981. Calculating solar radiation for ecological studies. Ecol. Modell. **14:** 1–19, doi:10.1016/0304-3800(81)90011-9

Bugenyi, F. W. B., and K. M. Magumba. 1996. The present physicochemical ecology of Lake Victoria, Uganda, p. 141–154. *In* T. C. Johnson and E. O. Odada [eds.], The limnology, climatology and paleoclimatology of the East African Lakes. Gordon and Breach.

Burling, M. C., G. N. Ivey, and C. B. Pattiaratchi. 1999. Convectively driven exchange in a shallow coastal embayment. Cont. Shelf Res. **19:** 1599–1616, doi:10.1016/S0278-4343(99)00034-5

Clark, C. O., P. J. Webster, and J. E. Cole. 2003. Interdecadal variability of the relationship between the Indian Ocean zonal mode and East African coastal rainfall anomalies. J. Clim. **16:** 548–554, doi:10.1175/1520-0442(2003)016<0548:IVOTRB>2.0.CO;2

Coulter, G. W., and R. H. Spigel. 1991. Hydrodynamics, p. 49–75. *In* G. W. Coulter [ed.], Lake Tanganyika and its life. Oxford Univ. Press.

Cozar, A., M. Bruno, N. Bergamino, B. Úbeda, L. Bracchini, A. M. Dattilo, and S. A. Loiselle. 2012. Basin-scale control on the phytoplankton biomass in Lake Victoria, Africa. PLoS One **7:** e29962, doi:10.1371/journal.pone.0029962

Crul, R. C. M. 1995. Limnology and hydrology of Lake Victoria. Studies and reports in hydrology 53. Comprehensive and comparative study of great lakes [Internet]. UNESCO/IHP-IV Project M-5.1. Available from http://ks360352.kimsufi.com/BIB/Publ_UNESCO/SR_053_1995.pdf

Dee, D. P., and others. 2011. The ERA-Interim reanalysis: Configuration and performance of the data assimilation system. Q. J. R. Meteorol. Soc. **137:** 553–597, doi:10.1002/qj.828

Dorostkar, A., and L. Boegman. 2013. Internal hydraulic jumps in a long, narrow lake. Limnol. Oceanogr. **58:** 153–172, doi:10.4319/lo.2013.58.1.0153

Eccles, D. H. 1974. An outline of the physical limnology of Lake Malawi (Lake Nyasa). Limnol. Oceanogr. **19:** 730–742, doi:10.4319/lo.1974.19.5.0730

Evans, J. H. 1961. A phytoplankton multi-sampler and its use in Lake Victoria. Nature **191:** 53–55, doi:10.1038/191053a0

Farrow, D. E., and J. C. Patterson. 1993. On the response of a reservoir sidearm to diurnal heating and cooling. J. Fluid Mech. **246:** 143–161, doi:10.1017/S0022112093000072

Fish, G. R. 1957. A seiche movement and its effect on the hydrology of Lake Victoria. Colonial Office Fishery Publications No. 10.

Gikumu-Njuru, P., R. E. Hecky, S. J. Guildford, and S. MacIntyre. 2013. Spatial variability of nutrient concentrations, fluxes, and ecosystem metabolism in Nyanza Gulf and Rusinga Channel, Lake Victoria (East Africa). Limnol. Oceanogr. **58:** 774–789, doi:10.4319/lo.2013.58.3.0774

Gill, A. E. 1982. Atmosphere-ocean dynamics. Academic Press.

Goyette, S., N. A. McFarlane, and G. M. Flato. 2000. Application of the Canadian regional climate model to the Laurentian Great Lakes region: Implementation of a lake model. Atmos.-Ocean **38:** 481–503, doi:10.1080/07055900.2000.9649657

Graham, M. 1929. The Victoria Nyanza and its fisheries. A report on the fishing surveys of Lake Victoria 1927–1928. Crown Agents for the Colonies.

Hecky, R. E. 1993. The eutrophication of Lake Victoria. Verh. Internat. Verein. Limnol. **25:** 39–48.

———, F. W. B. Bugenyi, P. Ochumba, J. F. Talling, R. Mugidde, M. Gophen, and L. Kaufman. 1994. Deoxygenation of the deep water of Lake Victoria, East Africa. Limnol. Oceanogr. **39:** 1476–1481, doi:10.4319/lo.1994.39.6.1476

———, R. Muggide, P. S. Ramlal, M. R. Talbot, and G. W. Kling. 2010. Multiple stressors cause rapid ecosystem change in Lake Victoria. Freshw. Biol. **55:** 19–42, doi:10.1111/j.1365-2427.2009.02374.x

Imberger, J. 1974. Natural convection in a shallow cavity with differentially heated end walls. Part 3. Experimental results. J. Fluid Mech. **65:** 247–260, doi:10.1017/S0022112074001376

———. 1985. The diurnal mixed layer. Limnol. Oceanogr. **30:** 737–770, doi:10.4319/lo.1985.30.4.0737

———, and J. C. Patterson. 1990. Physical limnology. Adv. Appl. Mech. **27:** 303–475, doi:10.1016/S0065-2156(08)70199-6

Ivey, G. N. 2004. Stratification and mixing in sea straits. Deep-Sea Res. II **51:** 441–453, doi:10.1016/j.dsr2.2003.07.020

Kalnay, E., and others. 1996. The NCEP/NCAR 40-year reanalysis project. Bull. Am. Met. Soc. **77:** 437–471, doi:10.1175/1520-0477(1996)077<0437:TNYRP>2.0.CO;2

Kanamitsu, M., W. Ebisuzaki, J. Woollen, S.-K. Yang, J. J. Hnilo, M. Fiorino, and G. L. Potter. 2002. NCEP-DOE AMIP-II reanalysis (R-2). Bull. Am. Meteorol. Soc. **83:** 1631–1643, doi:10.1175/BAMS-83-11-1631

Kitaka, G. E. B. 1971. An instance of cyclonic upwelling in the southern offshore waters of Lake Victoria. Afr, J. Trop. Hydrobiol. Fish. **2:** 85–92.

Kite, G. W. 1981. Recent changes in level of Lake Victoria. Hydrol. Sci. Bull. **26:** 233–243, doi:10.1080/02626668109490883

Kolding, J., P. van Zwieten, O. Mkumbo, G. Silsbe, and R. E. Hecky. 2008. Are the Lake Victoria fisheries threatened by exploitation or eutrophication? Towards an ecosystem-based approach to management. *In* G. Bianchi and H. R. Skjoldal [eds.], The Ecosystem Approach to Fisheries. CAB International.

Krishnamurthy, K. V., and A. M. Ibrahim. 1973. Hydrometeorological studies of Lakes Victoria, Kyoga and Albert, p. 272–277. *In* W. C. Ackermann, G. F. White, and E. B. Worthington [eds.], Man-made lakes: Their problems and environmental effects. Geophysical monograph No. 17. American Geophysical Union.

Laird, N. F., and D. A. R. Kristovich. 2002. Variations of sensible and latent heat fluxes from a Great Lakes buoy and associated synoptic weather patterns. J. Hydrometeorol. **3:** 3–12, doi:10.1175/1525-7541(2002)003<0003:VOSALH>2.0.CO;2

Lenters, J. D., T. K. Kratz, and C. J. Bowser. 2005. Effects of climate variability on lake evaporation: Results from a long-term energy budget study of Sparkling Lake, northern Wisconsin (USA). J. Hydrol. **308:** 168–195, doi:10.1016/j.jhydrol.2004.10.028

Liu, H., P. D. Blanken, T. Weidinger, A. Nordbo, and T. Vesala. 2011. Variability in cold front activities modulating cool-season evaporation from a southern inland water in the USA. Environ. Res. Lett. **6:** 024022, doi:10.1088/1748-9326/6/2/024022

Lofgren, B. M., and Y. Zhu. 2000. Surface energy fluxes on the Great Lakes based on satellite-observed surface temperatures 1992–1995. J. Great Lakes Res. **26:** 305–314, doi:10.1016/S0380-1330(00)70694-0

MacIntyre, S. 2013. Climatic variability, mixing dynamics, and ecological consequences in the African Great Lakes, p. 311–336. *In* C. R. Goldman, M. Kumagai, and R. D. Robarts [eds.], Climatic change and global warming of inland waters: Impacts and mitigation for ecosystems and societies. Wiley.

———, J. F. Clark, R. S. Jellison, and J. P. Fram. 2009. Turbulent mixing induced by non-linear internal waves in Mono Lake, CA. Limnol. Oceanogr. **54:** 2255–2272, doi:10.4319/lo.2009.54.6.2255

———, K. M. Flynn, R. Jellison, and J. R. Romero. 1999. Boundary mixing and nutrient fluxes in Mono Lake, California. Limnol. Oceanogr. **44:** 512–529, doi:10.4319/lo.1999.44.3.0512

———, A. Jonsson, M. Jansson, J. Aberg, D. E. Turney, and S. D. Miller. 2010. Buoyancy flux, turbulence, and the gas transfer coefficient in a stratified lake. Geophys. Res. Lett. **37:** L24604, doi:10.1029/2010GL044164

———, and J. M. Melack. 1982. Meromixis in an equatorial African soda lake. Limnol. Oceanogr. **27:** 595–609, doi:10.4319/lo.1982.27.4.0595

———, and ———. 2009. Mixing dynamics in lakes across climate zones, p. 603–612. *In* G. E. Likens [ed.], Encyclopedia of inland waters. Elsevier.

———, J. R. Romero, and G. W. Kling. 2002. Spatio-temporal variability in surface deepening and lateral advection in an embayment of Lake Victoria, East Africa. Limnol. Oceanogr. **47:** 656–671, doi:10.4319/lo.2002.47.3.0656

Maderich, V. S., G. J. F. van'Heust, and A. Brandt. 2001. Laboratory experiments on intrusive flows and internal waves in a thermocline. J. Fluid Mech. **432:** 285–311.

Melack, J. M., and P. Kilham. 1974. Photosynthetic rates of phytoplankton in East African alkaline, saline lakes. Limnol. Oceanogr. **19:** 743–755, doi:10.4319/lo.1974.19.5.0743

Meteorological Department of the East African High Commission (MDEAHC). 1959. The weather of East Africa during 1958.

———. 1960. The weather of East Africa during 1959.

———. 1961. The weather of East Africa during 1960.

———. 1962. The weather of East Africa during 1961.

———. 1963. The weather of East Africa during 1962.

———. 1964. The weather of East Africa during 1963.

———. 1965. The weather of East Africa during 1964.

———. 1966. The weather of East Africa during 1965.

———. 1967. The weather of East Africa during 1966.

———. 1968. The weather of East Africa during 1967.

———. 1969. The weather of East Africa during 1968.

———. 1970. The weather of East Africa during 1969.

———. 1971. The weather of East Africa during 1970.

———. 1972. The weather of East Africa during 1971.

———. 1973. The weather of East Africa during 1972.

———. 1974. The weather of East Africa during 1973.

———. 1975. The weather of East Africa during 1974.

———. 1976. The weather of East Africa during 1975.

———. 1977. The weather of East Africa during 1976.

———. 1978. The weather of East Africa during 1977.

———. 1979. The weather of East Africa during 1978.

———. 1980. The weather of East Africa during 1979.

———. 1981. The weather of East Africa during 1980.

———. 1982. The weather of East Africa during 1981.

———. 1983. The weather of East Africa during 1982

———. 1984. The weather of East Africa during 1983.

Millero, F. J., and A. Poisson. 1981. International one-atmosphere equation of state of seawater. Deep-Sea Res. **28:** 625–629.

Monismith, S. G., J. Imberger, and M. L. Morison. 1990. Convective motions in the sidearm of a small reservoir. Limnol. Oceanogr. **35:** 1676–1702, doi:10.4319/lo.1990.35.8.1676

Monteith, J. L. 1972. Solar radiation and productivity in tropical ecosystems. J. Appl. Ecol. **9:** 747–766, doi:10.2307/2401901

Mortimer, C. H., and W. Horn. 1982. Internal wave dynamics and their implications for plankton biology in the Lake of Zurich. Vierteljahrsschr. Nat. Ges. Zür. **127:** 299–318.

Nepf, H., and C. Oldham. 1997. Exchange dynamics of a shallow contaminated wetland. Aquat. Sci. **59:** 193–213, doi:10.1007/BF02523273

Newell, B. S. 1960. The hydrology of Lake Victoria. Hydrobiologia **15:** 363–383, doi:10.1007/BF00046419

Nicholson, S. E. 1996. A review of climate dynamics and climate variability in Eastern Africa, p. 25–56. *In* T. C. Johnson and E. O. Odada [eds.], The limnology, climatology and paleoclimatology of the East African Lakes. Gordon and Breach Publishers.

———, and X. Yin. 2002. Mesoscale patterns of rainfall, cloudiness, and evaporation over the Great Lakes of East Africa, p. 93–119. *In* E. O. Odada and D. O. Olago [eds.], The East African Great Lakes: Limnology, paleolimnology, and biodiversity. Kluwer.

Njuru, P. 2008. Physical and biogeochemical gradients and exchange processes in Nyanza Gulf and main Lake Victoria (East Africa). Ph.D. thesis. Univ. of Waterloo.

Ochumba, P. B. O. 1996. Measurement of water currents, temperature, dissolved oxygen and winds on the Kenyan Lake Victoria, p. 155–167. *In* T. C. Johnson and E. O. Odada [eds.], The limnology, climatology and paleoclimatology of the East African Lakes. Gordon and Breach.

Osborn, T. 1980. Estimates of the local rate of vertical diffusion from dissipation measurements. J. Phys. Oceanogr. **10:** 83–89, doi:10.1175/1520-0485(1980)010<0083:EOTLRO>2.0.CO;2

Otu, M., P. Ramlal, P. Wilkinson, R. I. Hall, and R. E. Hecky. 2011. Paleolimnological evidence of the effects of recent cultural eutrophication during the last 200 years in Lake Malawi, East Africa. J. Great Lakes Res. **37:** 61–74, doi:10.1016/j.jglr.2010.09.009

Patterson, G., M. J. Wooster, and C. B. Sear. 1998. Satellite-derived surface temperatures and the interpretation of the 3-dimensional structure of Lake Malawi, Africa: The presence of a profile-bound density current and the persistence of thermal stratification. Verh. Internat. Verein. Limnol. **26:** 252–255.

Ramlal, P. S., G. W. Kling, L. M. Ndawula, R. E. Hecky, and H. J. Kling. 2001. Diurnal fluctuations in P_{CO2}, DIC, oxygen and nutrients at inshore sites in Lake Victoria, Uganda, p. 67–82. *In* M. Munawar and R. E. Hecky [eds.], The great lakes of the world (GLOW): Food-web health and integrity. Backhuys.

Read, J. S., and others. 2012. Lake-size dependency of wind shear and convection as controls on gas exchange. Geophys. Res. Lett. **39:** L09405, doi:10.1029/2012GL051886

Rueda, F. J., and S. MacIntyre. 2010. Modelling the fate and transport of negatively buoyant storm-river water in small multi-basin lakes. Environ. Model. Softw. **25:** 146–157, doi:10.1016/j.envsoft.2009.07.002

Schmid, M., and others. 2007. Sources and sinks of methane in Lake Baikal: A synthesis of measurements. Limnol. Oceanogr. **52:** 1824–1837, doi:10.4319/lo.2007.52.5.1824

Schott, F., and J. Fernandez-Partagas. 1981. The onset of the summer monsoon during the FGGE 1979 experiment off the East African coast: A comparison of wind data collected by different means. J. Geophys. Res. **86:** 4173–4180, doi:10.1029/JC086iC05p04173

Song, Y. 2000. A numerical modeling study of the coupled variability of Lake Victoria in Eastern Africa and the regional climate. Ph.D. thesis. North Carolina State Univ.

———, F. H. Semazzi, L. Xie, and L. J. Ogallo. 2004. A coupled regional climate model for the Lake Victoria basin of East Africa. Internat. J. Climatol. **24:** 57–75, doi:10.1002/joc.983

———, F. H. M. Semazzi, and L. Xie. 2002. Development of a coupled regional climate simulation model for the Lake Victoria basin, p. 153–186. *In* E. O. Odada and D. O. Olago [eds.], The East African Great Lakes: Limnology, paleolimnology, and biodiversity. Kluwer.

Spigel, R. H., and G. W. Coulter. 1996. Comparison of hydrology and physical limnology of the East African Great Lakes: Tanganyika, Malawi, Victoria, Kivu and Turkana (with reference to some North American Great Lakes), p. 103–140. *In* T. C. Johnson and E. O. Odada [eds.], The limnology, climatology and paleoclimatology of the East African Lakes. Gordon and Breach.

Stainton, M. P., M. J. Capel, and F. A. J. Armstrong. 1977. The chemical analysis of fresh water, 2nd ed. Can. Fish. Mar. Serv. Misc. Spec. Publ. 25.

Talling, J. F. 1957. Diurnal changes of stratification and photosynthesis in some tropical African waters. Proc. R. Soc. B. **147:** 57–83, doi:10.1098/rspb.1957.0036

———. 1963. Origin of stratification in an African rift lake. Limnol. Oceanogr. **8:** 68–78, doi:10.4319/lo.1963.8.1.0068

———. 1966. The annual cycle of stratification and phytoplankton growth in Lake Victoria (East Africa). Int. Rev. Hydrobiol. **51:** 545–621, doi:10.1002/iroh.19660510402

———, and J. Lemoalle. 1998. Ecological dynamics of tropical inland waters. Cambridge Univ. Press.

Taylor, G. I. 1935. Statistical theory of turbulence. Proc. R. Soc. Lond. Ser. A **151:** 421–478, doi:10.1098/rspa.1935.0158

Tennekes, H., and J. L. Lumley. 1972. A first course in turbulence. MIT Press.

Turner, J. S. 1973. Buoyancy effects in fluids. Cambridge University Press.

Umlauf, L., and U. Lemmin. 2005. Interbasin exchange and mixing in the hypolimnion of a large lake: The role of long internal waves. Limnol. Oceanogr. **50:** 1601–1611, doi:10.4319/lo.2005.50.5.1601

Venayagamoorthy, S. K., and O. B. Fringer. 2007. On the formation and propagation of nonlinear internal boluses across a shelf break. J. Fluid Mech. **577:** 137–159, doi:10.1017/S0022112007004624

Verburg, P., J. P. Antenucci, and R. E. Hecky. 2011. Differential cooling drives large-scale convective circulation in Lake Tanganyika. Limnol. Oceanogr. **56:** 910–926, doi:10.4319/lo.2011.56.3.0910

———, and R. E. Hecky. 2003. Wind patterns, evaporation, and related physical variables in Lake Tanganyika, East Africa. J. Great Lakes Res. **29:** 48–61, doi:10.1016/S0380-1330(03)70538-3

Verschuren, D., and others. 2002. History and timing of human impact on L. Victoria. Proc. R. Soc. Lond. B. **269:** 289–294, doi:10.1098/rspb.2001.1850

Vidal, J., S. MacIntyre, E. E. McPhee-Shaw, W. J. Shaw, and S. G. Monismith. 2013. Temporal and spatial variability in the internal wave field of a lake with complex morphometry. Limnol. Oceanogr. **58:** 1557–1580, doi:10.4319/lo.2013.58.5.1557

Wells, M. G., and B. Sherman. 2001. Stratification produced by surface cooling in lakes with significant shallow regions. Limnol. Oceanog. **46:** 1747–1759, doi:10.4319/lo.2001.46.7.1747

Wolff, C., and others. 2011. Reduced interannual rainfall variability in East Africa during the last Ice Age. Science **333:** 743–747, doi:10.1126/science.1203724

Yeates, P. S., and J. Imberger. 2004. Pseudo two-dimensional simulations of internal and boundary fluxes in stratified lakes and reservoirs. Int. J. River Basin Manag. **1:** 1–23.

Yin, X., S. E. Nicholson, and M. B. Ba. 2000. On the diurnal cycle of cloudiness over Lake Victoria and its influence on evaporation from the lake. Hydrol. Sci. **45:** 407–424, doi:10.1080/02626660009492338

Associate editor: Craig L. Stevens

Received: 24 August 2013
Accepted: 14 April 2014
Amended: 20 June 2014